Am J Cancer Res 2024;14(4):1685-1711
www.ajcr.us /ISSN:2156-6976/ajcr0153976

Original Article

High glucose-induced NCAPD2 upregulation promotes malignant phenotypes and regulates EMT via the Wnt/β-catenin signaling pathway in HCC

Yuhua Mai[1], Chuanjie Liao[2,3], Shengyu Wang[4], Xin Zhou[5], Liheng Meng[1], Cuihong Chen[1], Yingfen Qin[1], Ganlu Deng[2,3]

[1]Department of Endocrinology, The First Affiliated Hospital of Guangxi Medical University, Nanning 530021, Guangxi, China; [2]Department of Oncology, The First Affiliated Hospital of Guangxi Medical University, Nanning 530021, Guangxi, China; [3]Key Laboratory of Early Prevention and Treatment for Regional High Frequency Tumor (Guangxi Medical University), Ministry of Education, Nanning 530021, Guangxi, China; [4]Department of Gastrointestinal Surgery, The First Affiliated Hospital of Guangxi Medical University, Nanning 530021, Guangxi, China; [5]Department of Hepatobiliary Surgery, The First Affiliated Hospital of Guangxi Medical University, Nanning 530021, Guangxi, China

Received October 18, 2023; Accepted March 29, 2024; Epub April 15, 2024; Published April 30, 2024

Abstract: Diabetes mellitus (DM) is recognized as a risk factor for hepatocellular carcinoma (HCC). High glucose levels have been implicated in inducing epithelial-mesenchymal transition (EMT), contributing to the progression of various cancers. However, the molecular crosstalk remains unclear. This study aimed to elucidate the molecular mechanisms linking DM to HCC. Initially, the expression of NCAPD2 in HCC cells and patients was measured. A series of functional in vitro assays to examine the effects of NCAPD2 on the malignant behaviors and EMT of HCC under high glucose conditions were then conducted. Furthermore, the impacts of NCAPD2 knockdown on HCC proliferation and the β-catenin pathway were investigated in vivo. In addition, bioinformatics methods were performed to analyze the mechanisms and pathways involving NCAPD2, as well as its association with immune infiltration and drug sensitivity. The findings indicated that NCAPD2 was overexpressed in HCC, particularly in patients with DM, and its aberrant upregulation was linked to poor prognosis. In vitro experiments demonstrated that high glucose upregulated NCAPD2 expression, enhancing proliferation, invasion, and EMT, while knockdown of NCAPD2 reversed these effects. In vivo studies suggested that NCAPD2 knockdown might suppress HCC growth via the β-catenin pathway. Functional enrichment analysis revealed that NCAPD2 was involved in cell cycle regulation and primarily interacted with NCAPG, SMC4, and NCAPH. Additionally, NCAPD2 was positively correlated with EMT and the Wnt/β-catenin pathway, whereas knockdown of NCAPD2 inhibited the Wnt/β-catenin pathway. Moreover, NCAPD2 expression was significantly associated with immune cell infiltration, immune checkpoints, and drugs sensitivity. In conclusion, our study identified NCAPD2 as a novel oncogene in HCC and as a potential therapeutic target for HCC patients with DM.

Keywords: Diabetes mellitus, hepatocellular carcinoma, EMT, NCAPD2, proliferation, metastasis

Introduction

Diabetes mellitus (DM), a disease characterized by chronic elevated blood glucose, had an estimated global prevalence of 9.3% (463 million people) in 2019, which is expected to rise to 10.2% (578 million people) by 2030 and 10.9% (700 million people) by 2045 [1]. This increasing incidence has made DM a significant global public health issue. Hepatocellular carcinoma (HCC) ranks as the fifth most common malignancy and the third leading cause of cancer-related mortality, with an annual global incidence of approximately 500,000 cases [2, 3]. Despite advances in the development and application of small-molecule multi-target tyrosine kinase inhibitors and immunotherapy allowing for improved survival, the prognosis for HCC patients remains poor, with a 5-year survival rate of only 12% [4]. Current evidences suggest that DM is an independent risk factor that significantly contributes to HCC progres-

https://doi.org/10.62347/HYNZ9211

sion [5]. Hyperglycemia adversely affects HCC progression and prognosis by regulating cell proliferation, metastasis, and drug resistance through multiple molecular mechanisms [6, 7]. However, the precise mechanisms by which DM contributes to HCC remain incompletely understood. Therefore, identifying new targets or signaling pathways with aberrant activation is urgently needed to prevent HCC development in DM patients and to improve the prognosis of HCC patients with DM.

Epithelial-mesenchymal transformation (EMT) is a crucial contributor for the malignant phenotype of tumor cells through facilitating various progression such as proliferation, metastasis, drug resistance, and cancer stemness [8]. The dysregulation of intercellular adhesion components, such as E-cadherin, N-cadherin, and vimentin, is a hallmark of EMT [9]. Multiple studies have demonstrated that high glucose conditions induce EMT, enhancing malignant behaviors in various cancers, including HCC [10-14]. Impaired inflammation and immunity, commonly observed in DM patients, diminish the response to chronic viral infections, such as hepatitis B, leading to HCC development. Cancer cells undergoing EMT have been shown to induce the production of pro-inflammatory cytokines, contributing to an aggressive phenotype switch. Moreover, in lung adenocarcinoma, high glucose-induced activation of EGFR/STAT3 signaling facilitated aggressive behaviors via EMT [15]. In HCC, hyperglycemia-activated c-Met induced mesenchymal phenotype acquisition, promoting HCC metastasis through metabolic reprogramming [16].

NCAPD2, a non-SMC subunit of condensin I located on chromosome 12p13.3, was initially found to play a crucial role in mitotic chromosome condensation and segregation, as well as neurological diseases [17, 18]. Recent studies have implicated NCAPD2 in the progression of colorectal cancer [19], breast cancer [20] and lung adenocarcinoma [21]. However, the role of NCAPD2 in HCC, particularly DM-related HCC, has not yet been reported. This study aimed to explore the expression and clinical significance of NCAPD2 in HCC patients with and without DM and to investigate the regulatory effect of NCAPD2 on the malignant phenotypes and EMT of HCC cells under high glucose conditions, along with the underlying molecular mechanisms of HCC and DM. Our study provides the first evidence that NCAPD2 is significantly overexpressed in HCC, especially in cases combined with DM. The upregulation of NCAPD2 was identified as a poor prognostic factor for HCC patients. High glucose levels upregulated NCAPD2 expression, while NCAPD2 knockdown attenuated the effects of high glucose, suggesting that NCAPD2 acts as a bridge between DM and HCC by regulating the Wnt/β-catenin-mediated EMT. Our findings reveal a novel mechanism contributing to the worsened prognosis observed in HCC patients with DM and offer a new potential therapeutic target for treating HCC patients.

Materials and methods

Tissue samples

A total of 56 pairs of fresh HCC tumor tissues and adjacent normal tissues were collected for total RNA isolation. These samples were obtained from patients at random undergoing surgery at the First Affiliated Hospital of Guangxi Medical University. Tissue samples were immediately stored in liquid nitrogen following detachment and subsequently stored in -80°C. For immunohistochemistry (IHC), 61 pairs formalin-fixed specimens were randomly collected at the First Affiliated Hospital of Guangxi Medical University. These specimens were then embedded in paraffin and stored at room temperature. All patients had been pathologically confirmed as HCC cases and had not received radiotherapy, chemotherapy, any targeted therapy, or immunotherapy prior to surgery. Clinicopathological parameters, including gender, age, height, weight, BMI, AFP, cirrhosis, vascular invasion, HBs antigen, Child-Pugh grade, T stage, N stage, M stage, and DM, of local HCC patients were obtained and analyzed with respect to different expression levels of NCAPD2. All specimens were routinely treated according to WHO classification for pathological diagnosis. The staging of patients was defined based on the TNM staging system (2017, version 8) developed by the American Joint Committee on Cancer (AJCC) and the Union for International Cancer Control (UICC). The inclusion criteria for patients with DM enrolled in this study were as follows: (1) a prior diagnosis of DM; (2) typical diabetes symptoms (polydipsia, polyuria, polyphagia, unexplained

weight loss) plus fasting plasma glucose concentration ≥ 7.0 mmol/L, an oral glucose tolerance test plasma glucose concentration ≥ 11.1 mmol/L, or a random intravenous plasma glucose concentration ≥ 11.1 mmol/L, or HbA1c ≥ 6.5%. All patients provided informed consent prior to sample collection, and the study protocol was approved by the institutional research Ethics Committee of the First Affiliated Hospital of Guangxi Medical University.

Quantitative real-time polymerase chain reaction (qRT-PCR)

Total RNA was extracted using Trizol (Invitrogen, Carlsbad, CA) or commercial RNA kit (Omega Bio-Tek, Norcross, GA, USA) according to the manufacturer's instructions. cDNA was synthetized using the MonScript™ kit (Monad Biotech, Suzhou, China). qRT-PCR was performed using SYBR Green PCR Master Mix (Monad Biotech). The primers used in this study are as follows: NCAPD2-F, 5'-TGGAGGGGTGAATCAGTATGT-3'; NCAPD2-R, 5'-GCGGGATACCACTTTTATCAGG-3'; GAPDH-F, 5'-CAACGTGTCAGTGGTGGACCTG-3'; GAPDH-R, 5'-GTGTCGCTGTTGAAGTCAGAGGAG-3'. The relative mRNA expression of NCAPD2 was quantitatively determined by the $2^{-\Delta\Delta Ct}$ method, with GAPDH serving as the internal control.

Cell culture

HCC cells (Huh7, SNU449, HepG2, and MHCC97H) and the human normal liver cell line L02 were obtained from Procell Life Science & Technology (Wuhan, China). Cells were cultured in Dulbecco's Modified Eagle Medium (DMEM, Gibco, USA) supplemented with 10% fetal bovine serum (FBS, Procell Life Science & Technology) and maintained at 37°C in a 5% CO_2 atmosphere, supplemented with 1% Penicillin-Streptomycin-Amphotericin B Solution (Solarbio, Beijing, China). For experiments involving high/low glucose conditions, cells were divided into a low glucose (LG) (DMEM with 5.6 mmol/L glucose) and high glucose (HG) group (DMEM with 25 mmol/L glucose).

Cell transfection

Small interfering RNAs (siRNAs) targeting NCAPD2 and a negative control (siNC) were designed by GenePharma (GenePharma, Shanghai, China).

The sense sequences were as follows: siNCAPD2#1, 5'-GGAGGAGAUUCCUGAGCAATT-3'; siNCAPD2#2, 5'-GGUACUGUCCAUCAAACAUTT-3'; siNCAPD2#3, 5'-GGUUCUCAGUGGCGAUCAATT-3'; and the siNC, 5'-UUCUCCGAACGUGUCACGUTT-3'. SiRNAs or the siNC were transfected into HCC cells using Lipofectamine 3000 (Thermo Fisher Scientific, USA) according to manufacturer's protocol. The transfection efficiency of siRNA vectors was assessed and confirmed by qRT-PCR and Western blot (Supplementary Figure 1A). siNCAPD2#1 and siNCAPD2#3 were selected for subsequent experiments.

Construction of NCAPD2 knockdown lentivirus and stably infection cells

For the stable knockdown of NCAPD2 expression in vivo experiments, short hairpin RNA targeting NCAPD2 was designed and synthesized by GenePharma (GenePharma, China) with a LV16 lentiviral vector. The target sequences for NCAPD2 shRNA were as follows: sh-NC, 5'-TTCTCCGAACGTGTCACGT-3', and sh-NCAPD2, 5'-GGAGGAGATTCCTGAGCAA-3'. Huh7 cells were infected with the lentivirus with an optimal multiplicity of infection (MOI) of 30 TU/mL following manufacturer's protocol. After 48 hours, transfected cells were selected with 0.5 ug/ml puromycin (Beyotime, Beijing, China) to establish stably transfected cell lines for further animal experiments. The knockdown efficiency of NCAPD2 in Huh7 cells was confirmed by qRT-PCR and Western blot.

Cell counting kit-8 (CCK-8) assay

CCK-8 kit (Biosharp, Anhui, China) was utilized to assess cell proliferation capacity. Forty-eight hours after transfection, cells were plated into 96-well plates at a final concentration of approximately 3×10^3 cells/well and cultured durations for 0 hour, 24 hours, 48 hours, and 72 hours. Subsequently, 10 μL of CCK-8 reagent was added to each well containing 90 μL DMEM, and the plates were incubated in a humidified incubator with 5% CO_2 at 37°C for 2 hours. The absorbance of the cell sample was measured at 450 nm.

Colony formation assay

HCC cells were harvested 48 hours after transfection, and 600 cells from each treatment were plated in a 6-well plate containing 2 ml of

culture medium, which was refreshed every two days. After 14 days of culture, the medium was discarded, and the colonies were washed thrice with PBS. The colonies were then fixed with 4% paraformaldehyde (PFA) for approximately 30 minutes and stained with 0.1% crystal violet for 30 minutes. Cultures were then washed with PBS, dried, and colonies were photographed and counted. This assay was performed in triplicate.

5-ethynyl-20-deoxyuridine (EdU) assay

An EdU kit (Beyotime) was utilized to evaluate the proliferative ability of HCC cells. After transfection with siRNA or the corresponding negative control, cells were cultured for 48 hours before splitting. Subsequently, cells (4×10^3 cells/Well) were seeded into 96-well plates and cultured for 24 hours. The plates were then incubated with EdU for 2 hours, fixed with 4% paraformaldehyde for 15 minutes, permeabilized with 0.3% Triton X-100 for 15 minutes, and stained with the reaction mixture in the dark at room temperature for 30 minutes. Nuclei were stained with Hoechst 33342. Representative images of EdU-positive cells were captured using fluorescence microscopy, and the percentages of EdU-positive cells were calculated. This assay was performed in triplicate.

Wound healing assay

The migratory ability of HCC cells was assessed using a wound healing assay. A line was drawn on the back of 6-well plates with a marker pen, perpendicular to the horizontal axis. Cells were cultured to 90% confluency, and a scratch was made along the marked line using a 200 μL pipette tip, perpendicular to the surface of plate. Subsequently, cells were cultured in DMEM containing 2% FBS and photographed after 48 hours using an inverted microscope. ImageJ software was used to calculate average scratch width. The migration rate was calculated by the formula: [(Denuded distance 0 h - Denuded distance at the endpoint)/Denuded distance 0 h].

Cell migration assay

A transwell migration assay was performed using an 8 μm pore chamber (Corning, Tewksbury, MA) to evaluate cell migration capability. Initially, 5×10^4 cells were seeded into the upper chamber in 100 μL DMEM without FBS, while the lower chamber was supplemented with 800 μL DMEM containing 10% FBS. After culture for 24 hours, cells remaining in the upper chamber were gently removed with a cotton swab. Cells that had migrated to the lower side of the membrane were fixed with 4% paraformaldehyde for 30 minutes and stained with 0.1% crystal violet for 20 minutes at room temperature. Migrated cells were then photographed and counted under the microscope. This assay was performed in triplicate.

Cell invasion assay

The cell invasion assay was performed using 24-well plates with 8 μm pore inserts (Corning) pre-coated with Matrigel (Abwbio, Shanghai, China). Cells were added to the top chamber and then grown in serum-free medium (7.0×10^4 cells/100 μl). 10% FBS was added to the bottom chamber as a chemoattractant. After 24 hours, cells that had invaded through the membrane were fixed with methanol, stained with 0.1% crystal violet for 20 minutes, and washed with PBS. Invasive cells were photographed using random fields and counted under the microscope in triplicate.

Western blot

Cells were harvested and total protein was extracted using RIPA buffer (Solarbio) supplemented with phenylmethanesulfonyl fluoride (PMSF, Solarbio). Thirty micrograms of protein from each sample were separated by 10% sodium dodecyl sulfate-polyacrylamide gel electrophoresis and transferred to PVDF membranes. The membranes were blocked with 5% milk at room temperature for 1 hour and incubated with primary antibodies overnight at 4°C. The primary antibodies used were as follows: NCAPD2 (1:1500, Proteintech, Wuhan, China), E-cadherin (1:20000, Proteintech), Vimentin (1:50000, Proteintech), N-cadherin (1:2000, Proteintech), β-catenin (1:5000, Proteintech), CyclinD1 (1:5000, Proteintech), c-Myc (1:2000, Proteintech) and GAPDH (1:5000, Proteintech). The membranes were then washed with TBST and incubated with an appropriate secondary antibody (1:5000, Proteintech). Blots were then washed thrice with TBST and bands were visualized with FluorChem M FM0593 system.

Protein expression levels were quantified and analyzed using ImageJ software, with GAPDH serving as the internal control.

Cellular immunofluorescence (IF)

Cells subjected to different treatments were cultured in 24-well plates on glass slides. After 48 hours, the cells were fixed with 4% paraformaldehyde and permeabilized with 0.5% Triton X-100 for 10 minutes. Cells were then blocked with 2% BSA for 1 hour and incubated with primary antibodies: Vimentin (1:600, Proteintech), E-cadherin (1:300, Proteintech), N-cadherin (1:300, Proteintech), and β-catenin (1:300, Proteintech) at 4°C overnight. The slides were then washed with PBS and incubated with fluorescent secondary antibodies (Alexa Fluor 488 or Alexa Fluor 555, Beyotime) for 1 hour. Nuclei were stained with DAPI. Representative images were captured under a fluorescence microscope, and fluorescence intensity was quantified using ImageJ for statistical analysis. Average fluorescence was calculated as the total fluorescence intensity of the region divided by the area of the regions.

Xenograft mouse model

A total of 10 healthy male BALB/c nude mice, aged 4-6 weeks, were provided by the Experimental Animal Center of Guangxi Medical University. Huh7-sh-NC and Huh7-sh-NCAPD2 cells (1×10^7) were resuspended in 100 μL of PBS and injected into the axilla of the mice (n = 5 per group) respectively. Three weeks' post-injection, the mice were euthanized by cervical dislocation, and the tumor weights were recorded. Tumor volume was calculated as: Volume (mm^3) = (length × width^2) × 0.5. Tumor tissues were collected and processed for histological evaluation. All animal experiments were approved by the Institutional Animal Care and Use Committee for medical laboratory animal sciences.

Immunohistochemistry (IHC)

Paraffin sections were baking at 60 deparaffinized in xylene, and hydrated through an ethanol gradient. After heat-induced antigen retrieval, the sections were blocked according to the instructions of the immunohistochemical detection kit (ZSGB-BIO, Beijing, China). Primary antibodies against NCAPD2 (1:200, Proteintech), β-catenin (1:1000, Proteintech) were incubated at 4°C overnight, followed by incubation with the corresponding secondary antibody for 1 hour at room temperature. DAB staining and hematoxylin counterstaining were performed. Images were captured under a microscope and analyzed. NCAPD2 expression levels were scored using the following formula: Immunohistochemical score (IHS) = staining percentage score × staining intensity score. The scoring criteria were based on positive percentage: 0% (0), ≤ 25% (1), 26-50% (2), 51-75% (3), > 75% (4); and intensity: negative (0), weakly positive (1), positive (2), strongly positive (3).

Expression and prognostic value of NCAPD2 in multiple public databases

The mRNA expression data for HCC were obtained from the ArrayExpress (https://www.ebi.ac.uk/arrayexpress/), GEO (https://portal.gdc.cancer.gov/), and The Cancer Genome Atlas (TCGA) (https://portal.gdc.cancer.gov/) databases. The UALCAN database (https://ualcan.path.uab.edu/index.html) was used to analyze differential expression and promoter methylation based on TCGA data. Clinical parameters (including gender, age, height, weight, BMI, pathologic T stage, pathologic N stage, pathologic M stage, pathologic stage, and histologic grade) of HCC patients were downloaded from TCGA database and then analyzed using UALCAN online or an R package across different NCAPD2 expression groups. Survival information of HCC patients from TCGA was obtained, and patients were stratified into high and low expression groups using the optimal cut-off determined by the Kaplan-Meier plotter database (http://kmplot.com/analysis/index.php?p=background). Kaplan-Meier curves were plotted to determine the prognostic value of NCAPD2 in HCC, with $P < 0.05$ considered statistically significant.

Pan-cancer analysis of NCAPD2 in public databases

The mRNA expression of NCAPD2 in more than 30 tumor and normal tissues was analyzed by using the TIMER database (https://cistrome.shinyapps.io/timer/). Different types of genetic alterations in the NCAPD2 gene in pan-cancer, including HCC, were analyzed using the cBioPortal (https://www.cbioportal.org/) database.

Tumor mutational burden (TMB) and TP53 mutation of NCAPD2 in HCC

Based on the RNA-seq data from TCGA, HCC patients were categorized into high and low NCAPD2 expression groups using the median value of NCAPD2 expression as the cutoff. Variants detected were categorized as base substitutions, insertions, or deletions. These variants, alongside the total exon length, were used to calculate the TMB. The differences in TMB between high and low NCAPD2 expression groups were illustrated using Waterfall Plots via the maftools package. Moreover, the expression level of NCAPD2 across different TP53 mutation statuses in HCC was analyzed using the UALCAN database.

Functional enrichment and protein-protein interaction (PPI) network construction of NCAPD2

The GeneMANIA database (https://genemania.org/) facilitates analysis and prediction of genes interacting with a selected gene based on shared functions. We utilized GeneMANIA database to identify similar functional genes which interact with NCAPD2, and a PPI network map was generated. To further investigate the potential biological functions of NCAPD2, we firstly used the GEPIA 2.0 database to identify genes related to NCAPD2. The top 300 related genes were listed and imported into the Metascape database (https://metascape.org/) for functional annotation and enrichment analysis. The biological functions involving NCAPD2 were predicted and visualized using Cytoscape.

Analysis of tumor immune microenvironment (TME) and immune cell infiltration

The Sangerbox website (http://www.sangerbox.com/home.html) was used to analyze the relationship between NCAPD2 expression, immune checkpoints (ICPs), and immune regulatory genes in multiple cancers. The infiltration proportions of 22 human immune cells in the TME were analyzed using CIBERSORT algorithms between high and low NCAPD2 expression groups. Additionally, the relationship between NCAPD2 and infiltration levels of immune cells in HCC, as well as ICPs, was analyzed using the TIMER database. The impact of different copy number alterations (CNAs) of NCAPD2 on immune cell infiltration levels was assessed using the TIMER database.

Pharmaceutical screening by NCAPD2

The pRRophetic R package (https://github.com/paulgeeleher/pRRophetic) was used to predict the sensitivity of commonly used antitumor drugs in groups with different NCAPD2 expressions. The half-maximal inhibitory concentration (IC_{50}) of targeted and chemotherapeutic agents for each HCC patient was predicted based on data from the GDSC database. $P < 0.001$ was considered statistically significant.

Statistical processing

All statistics are presented as mean ± standard deviation and were performed using GraphPad Prism 6.0. The t-test was used for statistical analysis between two independent groups, while one-way ANOVA was used for analyses involving more than two groups. Clinical parameters were analyzed using the Chi-square test. Spearman correlation analysis was applied for assessing drug sensitivity. $P < 0.05$ was considered statistically significant for in vitro experiments.

Results

NCAPD2 was upregulated in HCC and HCC combined with DM patients

We used qRT-PCR to assess the mRNA expression of NCAPD2 in 56 pairs HCC tissues and adjacent normal liver tissues. The results indicated that NCAPD2 expression was upregulated in 70% (39/56) HCC tumor tissues (**Figure 1A**), and the relative mRNA expression of NCAPD2 was significantly upregulated in tumor tissues as compared to the adjacent normal liver tissues ($P < 0.001$, **Figure 1B**). Subgroup analysis further distinguished between HCC patients with DM and those without. The mRNA expression of NCAPD2 was higher in HCC patients combined with DM (n = 17) than in those without DM (n = 39) ($P < 0.001$, **Figure 1C**).

IHC staining was utilized to investigate NCAPD2 protein expression. Representative IHC images demonstrated that NCAPD2 was primarily localized in the cytoplasm (**Figure 1D**). The expression of NCAPD2 exhibited a significantly stron-

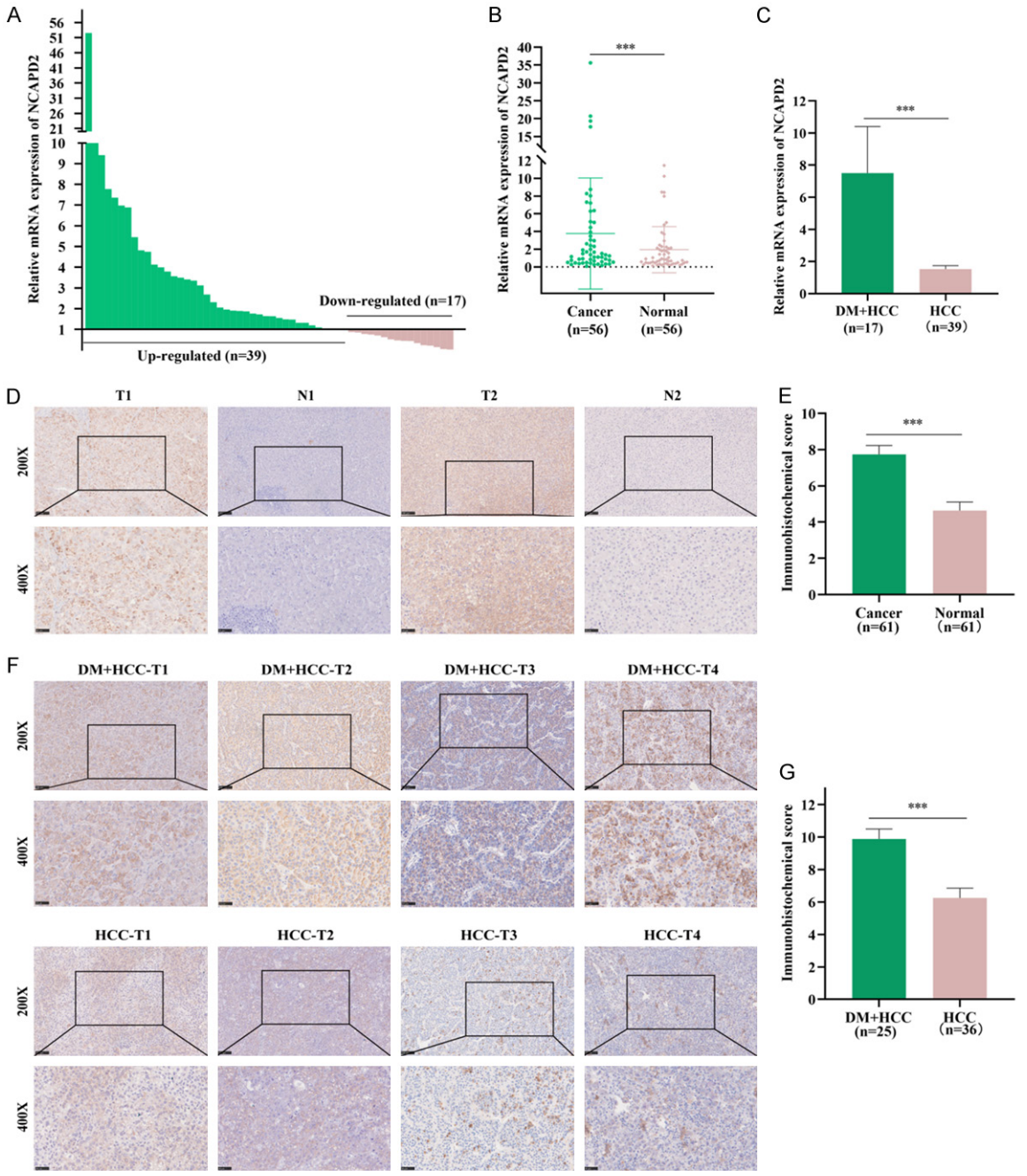

Figure 1. NCAPD2 was upregulated in HCC patients with or without DM. A. The relative mRNA expression level of NCAPD2 in each HCC patients. B. The mRNA expression of NCAPD2 compared in tumor and normal tissues of HCC patients. C. The mRNA expression of NCAPD2 in HCC patients with or without DM. D. Representative IHC pictures of NCAPD2 in tumor and adjacent normal tissues of HCC patients. E. IHC scores in HCC tumor and adjacent normal tissues. F. Representative IHC pictures of NCAPD2 in tumor tissues of HCC patients with or without DM. G. IHC scores in tumor tissues of HCC patients with or without DM. $^{***}P < 0.001$.

ger signal in tumors than in normal tissue (**Figure 1D**, **1E**, IHS: $P < 0.001$). Correspondingly, the IHC signal and IHS of NACPD2 were significantly higher in HCC combined with DM patients than those without DM (**Figure 1F**, **1G**, IHS: $P < 0.001$). These results implied an oncogenic role of NACPD2, highlighting its upregulation in HCC and its importance as a regulatory link between DM and HCC.

We further assessed the clinical significance of NCAPD2 by calculating the relationship

Table 1. Relationship between NCAPD2 mRNA expression and clinicopathological features of HCC patients

Characteristics	Low expression of NCAPD2	High expression of NCAPD2	*P* value
n	28	28	
Gender, n (%)			0.313
Male	24 (53.3%)	21 (46.7%)	
Female	4 (36.4%)	7 (63.6%)	
Age, n (%)			0.737
≤ 60	23 (51.1%)	22 (48.9%)	
> 60	5 (45.5%)	6 (54.5%)	
Weight, n (%)			0.577
≤ 60	11 (55.0%)	9 (45.0%)	
> 60	17 (47.2%)	19 (52.8%)	
Height, n (%)			0.284
< 165	11 (42.3%)	15 (57.7%)	
≥ 165	17 (56.7%)	13 (43.3%)	
BMI, n (%)			0.061
≤ 25	17 (63.0%)	10 (37.0%)	
> 25	11 (37.9%)	18 (62.1%)	
AFP (ng/mL), n (%)			0.589
≤ 200	17 (53.1%)	15 (46.9%)	
> 200	11 (45.8%)	13 (54.2%)	
Cirrhosis, n (%)			0.274
Absence	13 (59.1%)	9 (40.9%)	
Presence	15 (44.1%)	19 (55.9%)	
Vascular invasion, n (%)			1.000
Absence	20 (50.0%)	20 (50.0%)	
Presence	8 (50.0%)	8 (50.0%)	
HBsAg, n (%)			0.537
Negative	22 (52.4%)	20 (47.6%)	
Positive	6 (42.9%)	8 (57.1%)	
Child-Pugh grade, n (%)			1.000
A	27 (50.0%)	27 (50.0%)	
B	1 (50.0%)	1 (50.0%)	
T stage, n (%)			0.025*
T1-T2	27 (57.4%)	20 (42.6%)	
T3-T4	1 (11.1%)	8 (88.9%)	
N stage, n (%)			0.611
N0	25 (48.1%)	27 (51.9%)	
N1	3 (75.0%)	1 (25.0%)	
M stage, n (%)			1.000
M0	28 (50.9%)	27 (49.1%)	
M1	0 (0.0%)	1 (100%)	
DM, n (%)			< 0.001***
Absence	27 (69.2%)	12 (30.8%)	
Presence	1 (5.9%)	16 (94.1%)	

*$P < 0.05$, ***$P < 0.001$.

between NCAPD2 expression and clinicopathological characteristics. In cohort 1, HCC patients were divided into high- and low-NCAPD2 expression groups based on the median mRNA value of NCAPD2. As shown in **Table 1**, NCAPD2 mRNA expression was significantly associated with T stage ($P = 0.025$, **Table 1**) and the presence of DM ($P < 0.001$, **Table 1**). However, the mRNA expression of NCAPD2 was not associated with gender, age, weight, height, BMI, AFP, cirrhosis, vascular invasion, HBsAg, or Child-Pugh grade ($P > 0.05$, **Table 1**). For the protein expression of NCAPD2 in cohort 2, we defined the high NCAPD2 group as IHS ≥ 8 (n = 40) while the low NCAPD2 group was defined as IHS < 8 (n = 21). As shown in **Table 2**, NCAPD2 protein expression correlated significantly with age ($P = 0.016$, **Table 2**), T stage ($P = 0.021$, **Table 2**), and the presence of DM ($P < 0.001$, **Table 2**), but not with gender, BMI, AFP, cirrhosis, vascular invasion, HBsAg, and Child-Pugh grade ($P > 0.05$, **Table 2**). These results elucidated a crucial role of NCAPD2 in HCC especially in DM patients.

Expression and genetic alterations of NCAPD2 in pan-cancer

Given the differential expression and clinical value of NCAPD2 in our local cohort, we explored its role in public databases. The differential expression of NCAPD2 were analyzed across more than 30 human malignancies via the TIMER database. NCAPD2 was found to be significantly overexpressed in 13 tumor tissues, including HCC, compared to normal tissues, while the expression of NCAPD2 was downregu-

Table 2. Relationship between NCAPD2 protein expression and clinicopathological features of HCC patients

Characteristics	Low expression of NCAPD2	High expression of NCAPD2	*P* value
n	21	40	
Gender, n (%)			0.470
Male	19 (37.3%)	32 (62.7%)	
Female	2 (20.0%)	8 (80.0%)	
Age, n (%)			0.016*
≤ 60	18 (45.0%)	22 (55.0%)	
> 60	3 (14.3%)	18 (85.7%)	
Weight, n (%)			0.845
≤ 60	10 (35.7%)	18 (64.3%)	
> 60	11 (33.3%)	22 (66.7%)	
Height, n (%)			0.377
< 165	6 (27.3%)	16 (72.7%)	
≥ 165	15 (38.5%)	24 (61.5%)	
BMI, n (%)			0.947
≤ 25	14 (34.1%)	27 (65.9%)	
> 25	7 (35.0%)	13 (65.0%)	
AFP (ng/mL), n (%)			0.596
≤ 200	12 (50.0%)	20 (50.0%)	
> 200	9 (50.0%)	20 (50.0%)	
Cirrhosis, n (%)			0.142
Absence	12 (44.4%)	15 (55.6%)	
Presence	9 (26.5%)	25 (73.5%)	
Vascular invasion, n (%)			0.978
Absence	13 (35.1%)	24 (64.9%)	
Presence	8 (34.8%)	15 (65.2%)	
HBsAg, n (%)			0.608
Negative	15 (34.9%)	28 (65.1%)	
Positive	5 (29.4%)	12 (70.6%)	
Child-Pugh grade, n (%)			0.329
A	18 (32.1%)	38 (67.9%)	
B	3 (60.0%)	2 (40.0%)	
T stage, n (%)			0.021*
T1-T2	21 (40.4%)	31 (59.6%)	
T3-T4	0 (0.0%)	9 (100.0%)	
N stage, n (%)			1.000
N0	21 (35.0%)	39 (65.0%)	
N1	0 (0.0%)	1 (100.0%)	
M stage, n (%)			1.000
M0	21 (35.0%)	39 (65.0%)	
M1	0 (0.0%)	1 (100.0%)	
DM, n (%)			< 0.001***
Absence	19 (52.8%)	17 (47.2%)	
Presence	2 (8.0%)	23 (92.0%)	

*$P < 0.05$, ***$P < 0.001$.

lated significantly in thyroid cancer than normal tissues ($P < 0.05$, **Figure 2A**). To further elucidate the differential expression and the role of NCAPD2 in tumor progression, we then investigated the different types of genetic alterations of NCAPD2 in pan-cancer via the cBioPortal. The types of NCAPD2 gene alterations varied among cancers, with mutation being the most common in uterine corpus endometrial carcinoma (8.88%) and skin cutaneous melanoma (4.95%). Amplification was the second common alteration, observed in 6.71% of testicular germ cell tumors, 5.65% of ovarian serous cystadenocarcinoma, 5.26% of uterine carcinosarcoma, and 4.67% of brain lower grade glioma (**Figure 2B**).

TMB, TP53 mutation and genomic alterations of NCAPD2 in HCC

TMB plays a significant role in the prognosis and response to immunotherapy across numerous cancers. We further explored the mutation frequency of different genes within high and low NCAPD2 groups. Waterfall plots revealed the top 20 mutations, including TP53, CTNNB1, TTN, MUC16, and PCLO (**Figure 2C**, **2D**). Notably, the mutation frequency of TP53, a critical oncogene, was significantly higher in the high NCAPD2 expression group compared to the low NCAPD2 group (TP53: 38% vs 14%, **Figure 2C**, **2D**). However, the mutation frequency of CTNNB1, which is reported to be commonly mutated in HCC and associated with a reduced response to immunotherapy, was lower in NCAPD2-high group juxtaposed with the NCAPD2-low group (CTNNB1:

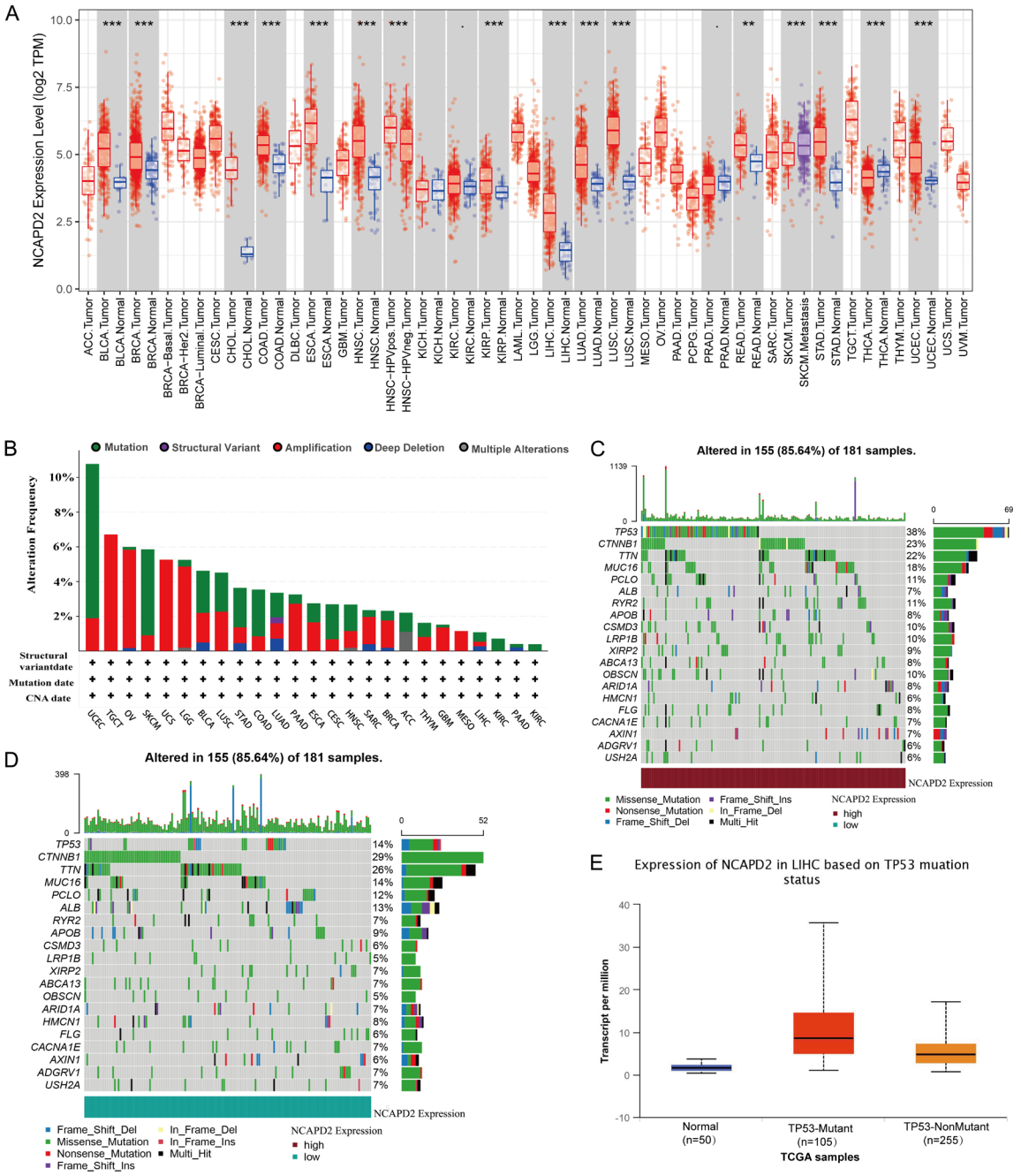
A
NCAPD2 Expression Level (log2 TPM)
B
Mutation
Structural Variant
Amplification
Deep Deletion
Multiple Alterations
Alteration Frequency
Structural variantdate
Mutation date
CNA date
C
Altered in 155 (85.64%) of 181 samples.
Missense_Mutation
Nonsense_Mutation
Frame_Shift_Del
Frame_Shift_Ins
In_Frame_Del
Multi_Hit
NCAPD2 Expression
high
low
D
Altered in 155 (85.64%) of 181 samples.
E
Expression of NCAPD2 in LIHC based on TP53 muation status
Transcript per million
Normal (n=50)
TP53-Mutant (n=105)
TP53-NonMutant (n=255)
TCGA samples
F
Samples per Patient
Mutation spectrum
TMB (nonsynonymous)
Mutation Count
Whole Genome Duplication
NCAPD2
Genetic Alteration
Missense Mutation (unknown significance)
Truncating Mutation (unknown significance)
Amplification
Deep Deletion
No alterations
C>A
C>G
C>T
T>A
T>C
T>G
No data
Mixed
no_wgd
wgd

Figure 2. Expression, genetic alteration and TMB of NCAPD2 in pan-cancer including HCC. A. NCAPD2 mRNA expression levels in pan-cancer from TCGA database via TIMER portal. B. Genetic alteration of NCAPD2 in pan-cancer from TCGA database via cBioPortal portal. C. Waterfall plots of the top 20 mutation genes in HCC patients with high NCAPD2. D. Waterfall plots of the top 20 mutation genes in HCC patients with low NCAPD2. E. The relationship between NCAPD2 expression and different TP53 mutant status in HCC patients. F. Type and frequency of NCAPD2 gene mutations in HCC. $^{*}P < 0.05$, $^{**}P < 0.01$, $^{***}P < 0.001$.

23% vs 29%, **Figure 2C**, **2D**). We then analyzed NCAPD2 expression levels across different TP53 mutation statuses, finding increased NCAPD2 expression in 105 HCC tumor samples with TP53 mutations compared to 255 samples without, according to TCGA data via the UALCAN portal ($P < 0.001$, **Figure 2E**). Furthermore, based on TCGA HCC samples, genomic alterations in NCAPD2 were observed in 6% of HCC patients (**Figure 2F**).

Upregulation and clinical values of NCAPD2 were validated in HCC patients in public databases

Following the aforementioned results of NCAPD2 in HCC, we used various public databases to validate the expression, clinical significance, and prognostic value of NCAPD2 in HCC. The upregulated mRNA expression of NCAPD2 was confirmed in the E_TABM_36 dataset from the ArrayExpress database ($P = 0.0045$, **Figure 3A**), GSE144269 ($P = 3.8e-13$, **Figure 3B**), GSE14520 ($P < 2.2e-16$, **Figure 3C**), and GSE54236 ($P = 3e-04$, **Figure 3D**) datasets from the GEO database, and the TCGA HCC dataset ($P < 1e-12$, **Figure 3E**), supporting the aberrant expression of NCAPD2 in our local HCC specimens.

Clinicopathological parameters of HCC patients were downloaded from the TCGA database. A total of 371 HCC patients were divided into high and low NCAPD2 groups based on the median value of NCAPD2 mRNA expression. As shown in **Table 3**, we found that the expression of NCAPD2 was significantly associated with patient age ($P = 0.005$), weight ($P = 0.009$), BMI ($P = 0.042$), pathological T stage ($P = 0.007$), pathological stage ($P = 0.001$), and histologic grade ($P < 0.001$), but not with gender ($P = 0.065$), height ($P = 0.098$), pathological N stage ($P = 0.394$), or pathological M stage ($P = 0.279$). Additionally, NCAPD2 expression levels correlated with tumor grade, cancer stages, and nodal metastasis status in the UALCAN database (**Figure 3F-H**). The methylation of the NCAPD2 DNA promoter was lower in HCC than in normal tissues (**Figure 3I**).

Prognostic value of NCAPD2 in HCC

Survival information from HCC patients was used to generate Kaplan-Meier survival curves from the K-M plotter database, to elucidate the relationship between NCAPD2 and HCC prognosis. Patients with high NCAPD2 expression exhibited shorter Overall Survival (OS: 25.2 m vs 70.5 m, HR = 2.08 [1.46-2.96], $P = 3e-05$) and Recurrence-Free Survival (RFS: 15.07 m vs 34.4 m, HR = 1.63 [1.16-2.31], $P = 0.005$) compared to those with low expression (**Figure 3J**, **3K**). Progression-Free Survival (PFS: 12.87 m vs 29.77 m, HR = 1.65 [1.23-2.22], $P = 0.00079$) and Disease-Specific Survival (DSS: 49.67 m vs 84.4 m, HR = 2.39 [1.52-3.74], $P = 8.9e-05$) also showed similar trends (**Figure 3L**, **3M**), indicated that NCAPD2 was both overexpressed in HCC tumor tissues and acted as a key regulator of HCC progression, supporting the results of our local HCC specimens.

High glucose induced the expression of NCAPD2 in HCC

Given the notable overexpression of NCAPD2 and its significant clinical implications in HCC, with and without DM, we investigated the impact of NCAPD2 on HCC cells under high glucose in vitro. The expression of NCAPD2 in HCC cell lines compared to normal liver epithelial cell line LO2 was detected by qRT-PCR and Western blot. Results demonstrated that both mRNA and protein expression of NCAPD2 in HCC cell lines (Huh7, SNU449, HepG2 and MHCC97H) were upregulated compared to LO2 ($P < 0.001$, **Figure 4A**, **4B**). SNU449 and Huh7 cells, with the highest NCAPD2 expression, were selected for further study. Cells were cultured in LG (5.6 mmol/L) or HG (25 mmol/L) and harvested at different timepoints. qRT-PCR assay demonstrated a time-dependent increase NCAPD2 mRNA expression in cells culture in HG compared with LG (Supplementary Figure 1B). The 48 hours mark was selected for further evaluation. The CCK-8 assay indicated that HG conditions significantly promoted the growth of Huh7 and SNU449 cells at 24 hours, 48 hours, and 72 hours juxtaposed with LG ($P <$

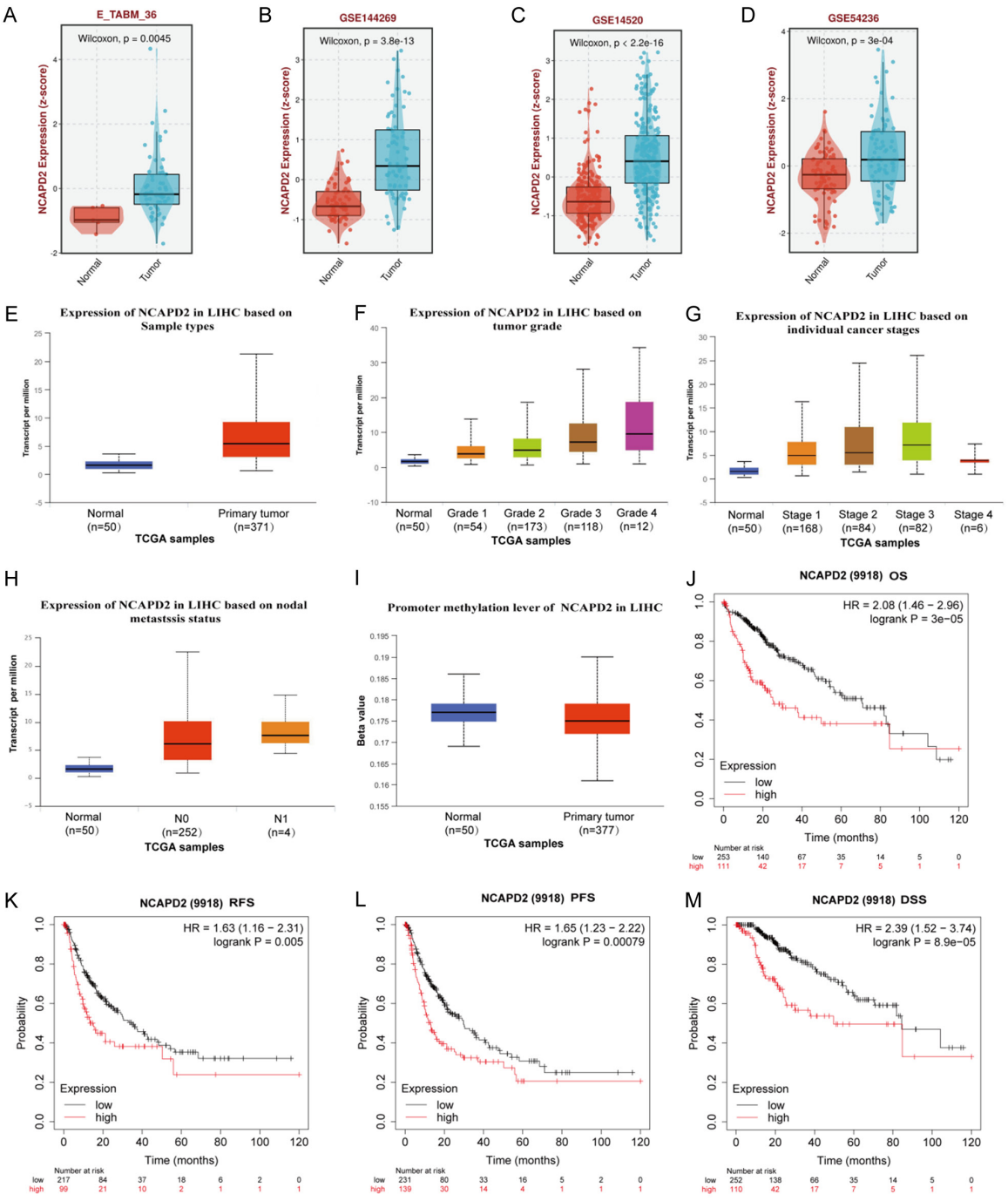

Figure 3. Expression profile, clinical and prognostic values of NCAPD2 in HCC patients from public databases. A-E. Expression profiles of NCAPD2 in HCC tumor and normal tissues from ArrayExpress, GEO and TCGA databases. F-H. Expression profiles of NCAPD2 in HCC patients stratified based on tumor grade, stage and nodal metastasis criteria. I. DNA promoter methylation of NCAPD2 in HCC tumor and normal tissues. J-M. The K-M curves of OS, RFS, PFS and DSS in HCC patients with high and low NCAPD2 expression.

0.001, **Figure 4C**). qRT-PCR and Western blot results confirmed that mRNA and protein levels of NCAPD2 were significantly higher in the HG groups compared to the LG groups ($P < 0.001$, **Figure 4D**, **4E**), showing that high glucose upregulated NCAPD2 expression in HCC cells.

Table 3. Relationship between NCAPD2 expression and clinicopathological parameters of HCC patients from TCGA database

Characteristics	Low expression of NCAPD2	High expression of NCAPD2	*P* value
n	185	186	
Gender, n (%)			0.065
Female	52 (43.0%)	69 (57.0%)	
Male	133 (53.2%)	117 (46.8%)	
Age, n (%)			0.005**
≤ 60	75 (42.4%)	102 (57.6%)	
> 60	110 (57.0%)	83 (43.0%)	
Weight, n (%)			0.009**
≤ 70	80 (44.0%)	102 (56.0%)	
> 70	94 (58.0%)	68 (42.0%)	
Height, n (%)			0.098
≤ 170	101 (47.8%)	115 (52.2%)	
> 170	69 (56.1%)	54 (43.9%)	
BMI, n (%)			0.042*
≤ 25	80 (45.2%)	97 (54.8%)	
> 25	89 (56.3%)	69 (43.7%)	
Pathologic T stage, n (%)			0.007**
T1	105 (58.0%)	76 (42.0%)	
T2	43 (45.7%)	51 (54.3%)	
T3	29 (36.2%)	51 (63.8%)	
T4	5 (38.5%)	8 (61.5%)	
Pathologic N stage, n (%)			0.394
N0	117 (46.4%)	135 (53.6%)	
N1	1 (25%)	3 (75%)	
Pathologic M stage, n (%)			0.279
M0	127 (47.7%)	139 (52.3%)	
M1	3 (75%)	1 (25%)	
Pathologic stage, n (%)			0.001**
Stage I	98 (57.3%)	73 (42.7%)	
Stage II	40 (46.5%)	46 (53.5%)	
Stage III	28 (32.9%)	57 (67.1%)	
Stage IV	4 (80%)	1 (20%)	
Histologic grade, n (%)			< 0.001***
G1	38 (69.1%)	17 (30.9%)	
G2	98 (55.4%)	79 (44.6%)	
G3	43 (35.2%)	79 (64.8%)	
G4	4 (33.3%)	8 (66.7%)	

*$P < 0.05$, **$P < 0.01$, ***$P < 0.001$.

High glucose promoted malignant behaviors and EMT in HCC cells

EdU assay was performed to evaluate the effects of HG conditions on the proliferation abilities of HCC cells. The EdU assay revealed a significantly higher EdU positive rate in Huh7 and SNU449 cells treated with HG ($P < 0.001$, **Figure 5A**). Transwell migration and wound healing assays were performed to evaluate migration ability. Results indicated that HG conditions enhanced the migration ability of HCC cells, with a greater number of migrated cells and a longer healing distance than cells in LG groups ($P < 0.01$, **Figure 5B**, **5C**). The Transwell invasion assay demonstrated a stronger invasion capability in HG groups than those in LG groups ($P < 0.001$, **Figure 5B**).

Previous studies have shown that high glucose induces EMT in multiple cancer cells. We examined the EMT status under our HG condition. Western blot analysis of EMT biomarkers confirmed the initiation of EMT in HCC cells treated with HG, accompanied with the upregulation of mesenchymal markers (Vimentin, N-cadherin) and the downregulation of epithelial biomarkers (E-cadherin) (**Figure 5D**). Cellular co-location IF staining with E-cadherin, Vimentin, and N-cadherin corroborated Western blot results ($P < 0.001$, **Figure 5E**).

Knockdown of NCAPD2 attenuated the effects on malignant behaviors and EMT promoted by HG

We conducted in vitro experiments to determine whether NCAPD2 regulate the biological effects exerted by HG. SiRNAs targeting NCAPD2 (siNCAPD2) and a corresponding negative control (siNC) were designed and transfected into Huh7 and SNU449 cells. qRT-PCR and Western blot confirmed the transfection efficiency in both HCC cells ($P < 0.001$, **Figure 6A**, **6B**). HCC cells were then cultured in HG. Knockdown of NCAPD2 resulted in weakened proliferative ability at 24 hours, 48 hours, and

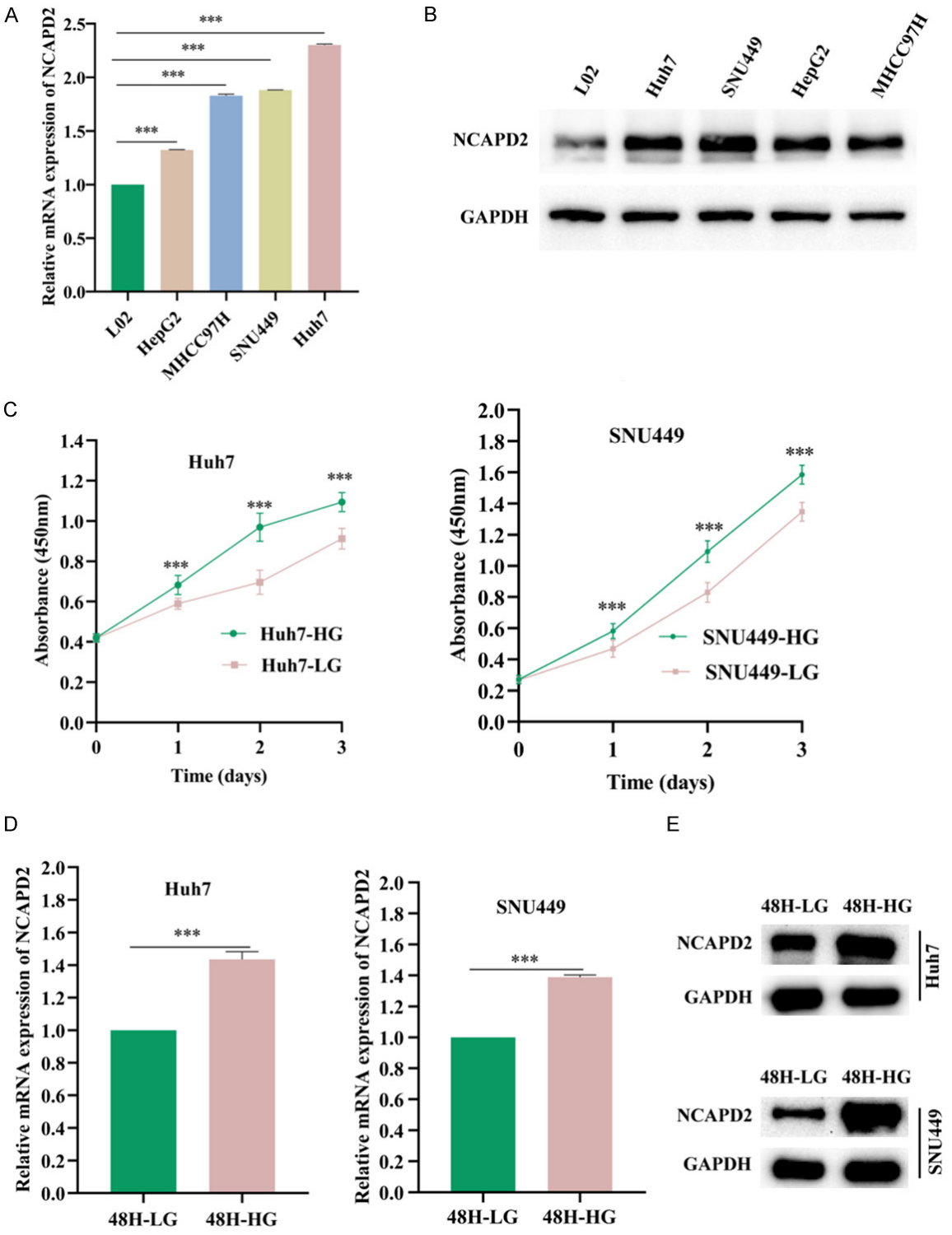

Figure 4. High glucose upregulated the expression of NCAPD2. A. The relative mRNA expression of NCAPD2 in different HCC cells and normal liver cell L02. B. The protein expression of NCAPD2 in different HCC cells and normal liver cell L02. C. CCK-8 assay detected the cell viability of HCC cells treated with different concentration of glucose. D, E. The mRNA and protein expression of NCAPD2 in HCC cells treated with high glucose. $^{***}P < 0.001$.

72 hours compared to the negative control groups ($P < 0.001$, **Figure 6C**). The number of EdU positive cells and formed colonies were significantly lower in the siNCAPD2 groups than

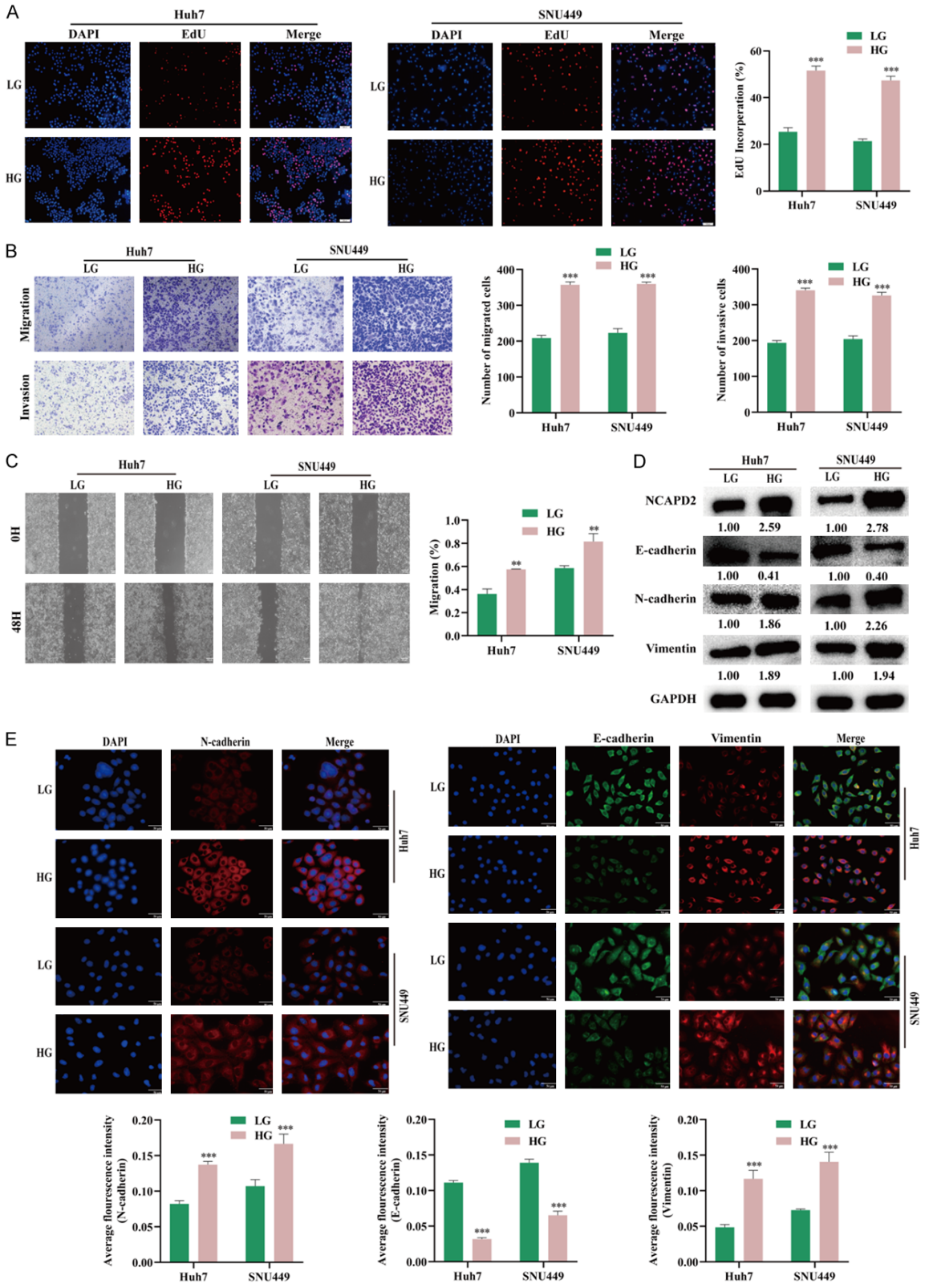

Figure 5. High glucose promoted the malignant phenotypes and EMT of HCC cells. A. EdU assay detected the proliferation of HCC cells treated with different concentration of glucose. B. Transwell migration (upper) and invasion (lower) assays reflected the migrative and invasive abilities of HCC cells in different concentration of glucose. C. Wound healing assay explored the effects of high and low glucose on HCC migration. D. EMT-related markers detected by Western blot in HCC cells treated with different concentration of glucose. E. Cellular IF reflected the co-location and expression of E-cadherin, Vimentin and N-cadherin in HCC cells treated with different concentration of glucose. $^{**}P < 0.01$, $^{***}P < 0.001$.

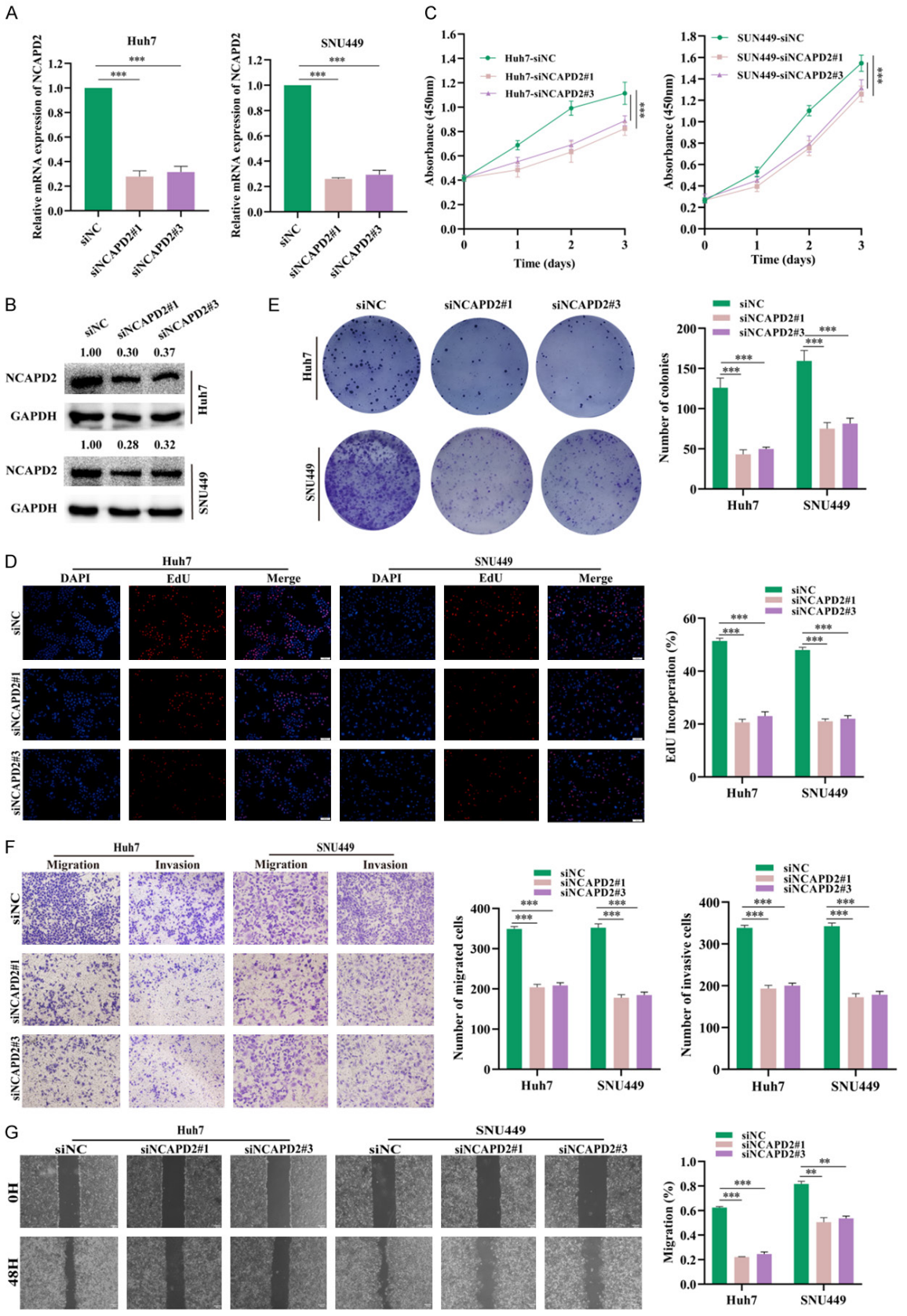

Figure 6. Knockdown of NCAPD2 reversed the effects on malignant phenotypes of HCC cells induced by high glucose. A, B. The transfected efficiency of NCAPD2 was confirmed by qRT-PCR and Western blot. C-E. Knockdown of

NCAPD2 inhibited the proliferation in HCC cells subjected into high glucose condition by CCK-8 (C), EdU (D) and colony formation (E) assays. F, G. Knockdown of NCAPD2 inhibited the migration and invasion in HCC cells subjected into high glucose condition by transwell migration/invasion (F) and wound healing (G) assays. $^{**}P < 0.01$, $^{***}P < 0.001$.

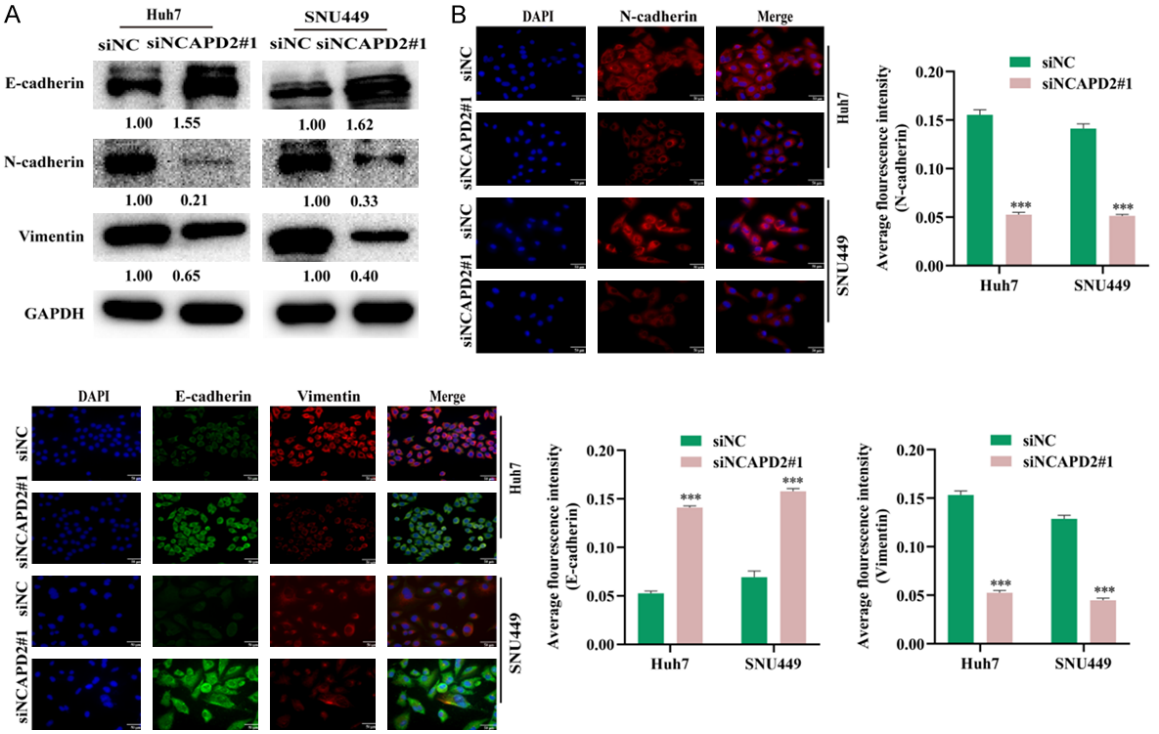

Figure 7. Knockdown of NCAPD2 reversed the effects on EMT of HCC cells induced by high glucose. A, B. Knockdown of NCAPD2 inhibited the EMT in HCC cells subjected into high glucose condition by Western blot (A) and IF (B) assays. $^{***}P < 0.001$.

in the siNC groups ($P < 0.001$, **Figure 6D**, **6E**). The migration and invasion capacities were also significantly reduced in the siNCAPD2 groups compared to the siNC groups ($P < 0.001$, **Figure 6F**), as well as the healing rate ($P < 0.01$, **Figure 6G**). These results suggested that knockdown of NCAPD2 suppressed the proliferation, migration, and invasion of HCC cells cultured in HG.

We further investigated whether NCAPD2 is involved in HG-induced EMT. As shown in **Figure 7A** and **7B**, EMT biomarkers detected by Western blot and IF revealed that NCAPD2 knockdown led to an increased expression of epithelial biomarker E-cadherin and a decreased expression of mesenchymal markers (Vimentin, N-cadherin), suggesting that NCAPD2 reversed the EMT induced by HG condition.

Functional enrichment and PPI network of NCAPD2

To better understand the underlying functions and mechanisms of NCAPD2 in cancer, we used the GeneMANIA database to identify genes with similar functions and potential interactions with NCAPD2. The PPI network of NCAPD2 was established with GeneMANIA, suggesting potential interactions between NCAPD2 and genes such as NCAPG, SMC4, NCAPH, SMC2, NCAPD3, CSNK2A1, and CSNK2A2 (**Figure 8A**). To further explore the potential biological function of NCAPD2, we screened the top NCAPD2-related 300 genes using the GEPIA 2.0 database. Functional enrichment indicated that NCAPD2 might be involved in positively regulating the cell cycle (**Figure 8B**, **8C**). The five most enriched functions included the mitotic cell cycle, cell cycle, regulation of cell

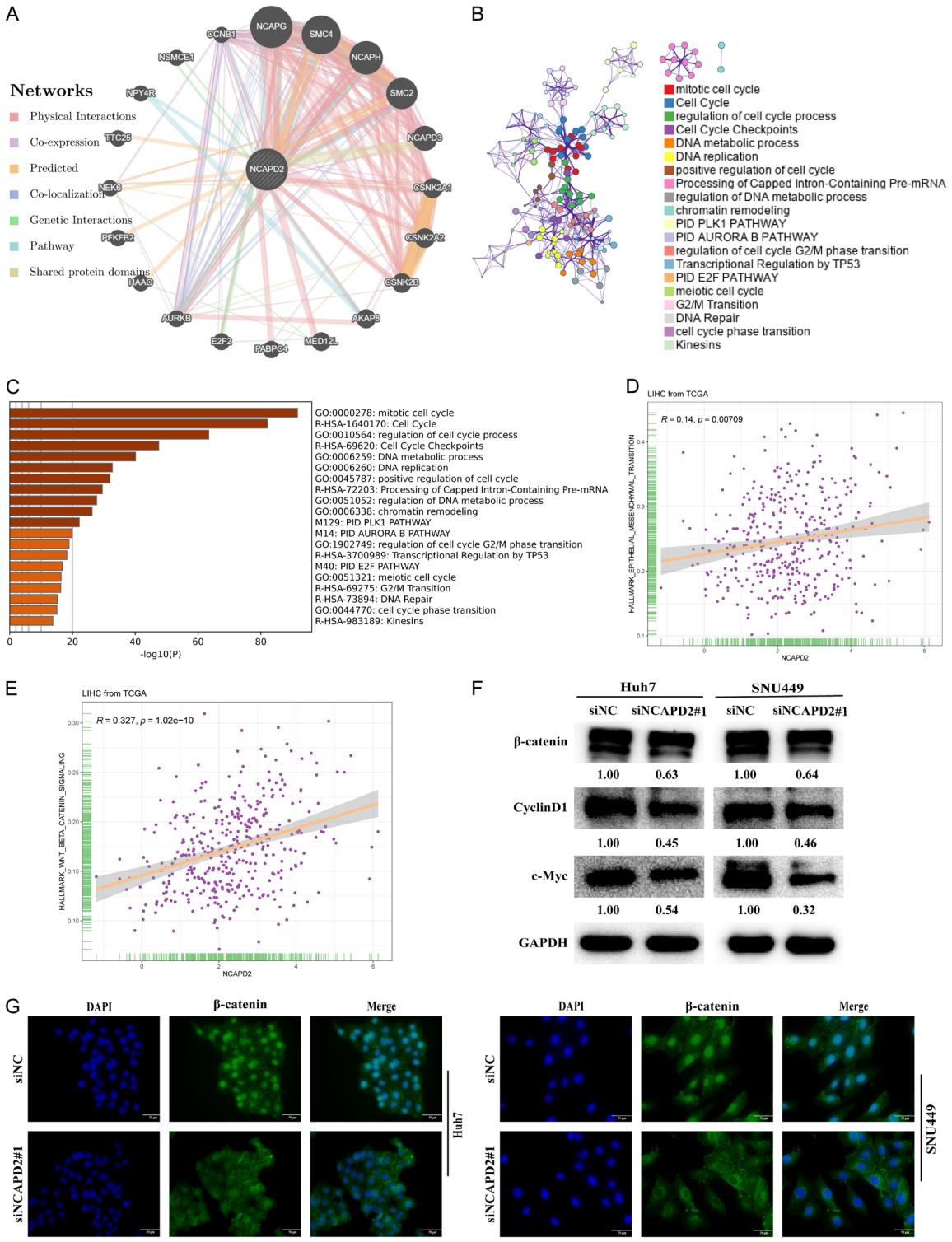

Figure 8. PPI and functional enrichment analysis of NCAPD2. A. PPI network of NCAPD2 and interacted genes via GeneMANIA. B, C. Metascape analysis of the potential biological functions of NCAPD2 in HCC. D, E. NCAPD2 expression was positively correlated with EMT (D) and Wnt/β-catenin pathway (E). F. Knockdown of NCAPD2 inhibited the protein expression of Wnt/β-catenin pathway. G. The entry of β-catenin into the nucleus decreased after NCAPD2 knockdown.

cycle processes, cell cycle checkpoints, and DNA metabolic process (**Figure 8B**, **8C**).

Given that NCAPD2 knockdown inhibited proliferation, motility, and EMT in HCC cells, and con-

sidering NCAPG, the most likely interacting gene in the PPI network, regulates EMT via the Wnt/β-catenin pathway, combining the important role of Wnt/β-catenin pathway in EMT, we explored the relationship of NCAPD2 with key components of EMT and the Wnt/β-catenin pathway. NCAPD2 showed positive correlations with EMT (r = 0.14, *P* = 0.007, **Figure 8D**) and Wnt/β-catenin pathway (r = 0.327, *P* = 1.02e-10, **Figure 8E**), indicating that NCAPD2 may regulate EMT through the Wnt/β-catenin pathway in HCC cells. Western blot analysis confirmed that NCAPD2 downregulation inhibited the expression of β-catenin, CyclinD1, and c-Myc in Huh7 and SNU449 cells (**Figure 8F**). Additionally, cellular IF indicated a significant reduction in nuclear β-catenin following NCAPD2 knockdown (**Figure 8G**), suggesting that NCAPD2 may regulate HCC progression through the Wnt/β-catenin pathway.

Knockdown of NCAPD2 suppressed HCC progression in vivo

To further confirm the role of NCAPD2 in promoting HCC proliferation and regulating the Wnt/β-catenin pathway, we established a xenograft subcutaneous model by stably infecting Huh7 cells with NCAPD2 shRNA lentivirus (sh-NCAPD2 group) or negative control shRNA lentivirus (sh-NC group). Knockdown efficiency was verified by qRT-PCR and Western blot (*P* < 0.001, **Figure 9A**, **9B**). After 21 days of implantation, mice in the sh-NC group exhibited significantly larger tumor volumes and weights compared to the sh-NCAPD2 group (*P* < 0.001, **Figure 9C**). Additionally, tumor tissues in sh-NC group displayed higher expression of Ki67, β-catenin, and NCAPD2 compared to tumor tissues from the sh-NCAPD2 groups (**Figure 9D**). These results suggested that downregulation of NCAPD2 inhibited the growth of HCC cells in vivo through the Wnt/β-catenin pathway.

TME and immune cell infiltration analysis of NCAPD2

Given the significant impact of immune response on patient prognosis and treatment decision, we focused on the relationship between NCAPD2 and tumor immune microenvironment, which is considered to be a key regulator in immunotherapy response. We explored the pan-cancer correlation between NCAPD2 and multiple immunomodulatory genes, including immune checkpoints, chemokines, chemokine receptors, MHCs, immunosuppressors, and immune activators.

We found that the expression of NCAPD2 was significantly correlated with immune checkpoint genes and immunomodulatory genes in a variety of cancers (**Figure 10A**, **10B**). Specifically, in HCC, 56 out of 60 immune checkpoint genes, such as the stimulatory HMGB1, TNFSF4, and TLR4, were significantly positively correlated with NCAPD2 expression (r > 0, *P* < 0.05, **Figure 10A**). Furthermore, we found that NCAPD2 expression was positively correlated with immunomodulatory genes in a pan-cancer analysis (r > 0, *P* < 0.05, **Figure 10B**). In HCC, a total 133 out of 150 immunomodulatory genes were associated with NCAPD2 expression, especially chemokines and chemokine receptors such as CX3CL1, CXCL16, CXCL5, and IL6R (*P* < 0.05, **Figure 10B**).

Immune cells play a crucial role in shaping the immune microenvironment. To evaluate the infiltration landscape of 22 tumor microenvironment (TME) cells between high and low NCAPD2 expression in HCC, we utilized the CIBERSORT algorithm. Significant differences in immune cell infiltration were observed between groups with differing NCAPD2 expression levels. High NCAPD2 expression was associated with infiltration levels of monocytes (*P* < 0.05, **Figure 10C**) and resting mast cells (*P* < 0.05, **Figure 10C**). Furthermore, the correlation between NCAPD2 and ICPs (PDCD1 and CTLA4), as well as immune cells, was analyzed using the TIMER database. We found that NCAPD2 positively correlated with PDCD1 (r = 0.356, *P* < 0.001, **Figure 10D**) and CTLA4 (r = 0.318, *P* < 0.001, **Figure 10E**). Additionally, NCAPD2 expression showed significantly positive correlations with dendritic cells (r = 0.525, *P* < 0.001, **Figure 10F**), macrophages (r = 0.497, *P* < 0.001, **Figure 10F**), B cells (r = 0.473, *P* < 0.001, **Figure 10F**), neutrophils (r = 0.446, *P* < 0.001, **Figure 10F**), CD4+ T cells (r = 0.426, *P* < 0.001, **Figure 10F**), and CD8+ T cells (r = 0.369, *P* < 0.001, **Figure 10F**). Moreover, the impact of CNA types and the infiltration levels of immune cells were investigated to elucidate the underlying mechanism of NCAPD2-involved immune cell infiltration. Arm-level deletion of NCAPD2 significantly influenced the infiltration levels of B cells, CD8+ T cells, and dendritic cells (*P* < 0.05, **Figure 10G**). These results indicated that NCAPD2 served as

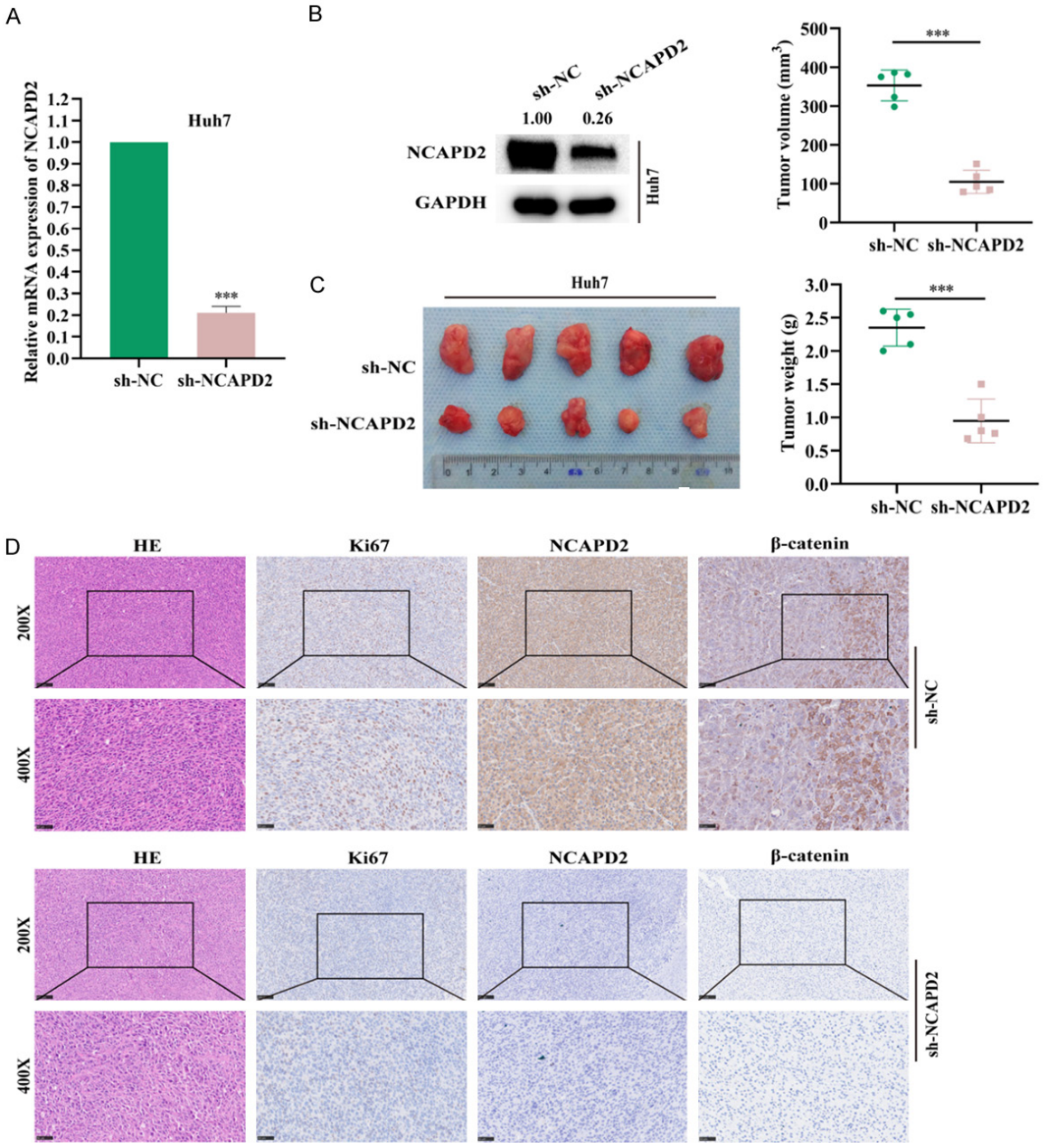

Figure 9. Down-regulation of NCAPD2 suppressed HCC progression in vivo. The xenograft subcutaneous model was constructed by stably infecting Huh7 cells with sh-NCAPD2 or sh-NC. A, B. qRT-PCR and Western blot analysis confirmed the efficiency of NCAPD2 knockdown by shRNA in vivo in Huh7 cells. C. Tumor volume and tumor weight of xenograft tumors in two groups were measured (n = 5). D. Representative images of HE, Ki67, NCAPD2 and β-catenin expression in tumors from a xenograft subcutaneous model detected by IHC staining. ***$P < 0.001$.

a pivotal regulator in the immune microenvironment of HCC through arm-level deletion.

Relationship between NCAPD2 expression and drug sensitivity

To improve the clinical practicability of NCAPD2, we explored its pharmaceutical implications by predicting the IC_{50} of anti-cancer drugs between high and low NCAPD2 expression groups. As shown in **Figure 11**, NCAPD2 expression was negatively associated with the efficacy of most anticancer drugs, including Sorafenib, XL-184, Sunitinib, Doxorubicin, Paclitaxel, Vinorelbine, Obatoclax ($P < 0.001$, **Figure 11A-T**), suggesting that these drugs, commonly used in HCC

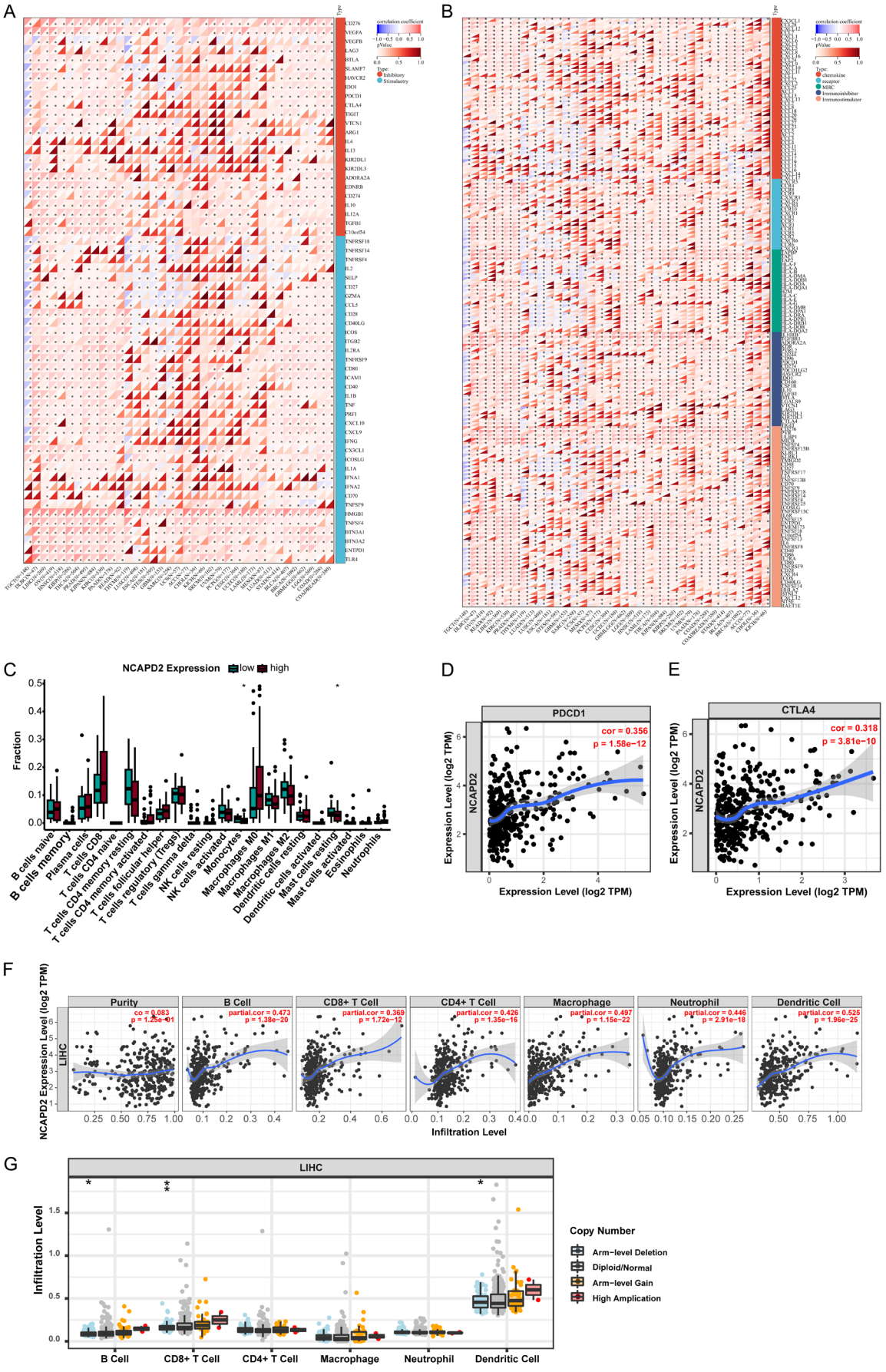
A
B
C
NCAPD2 Expression
low
high
Fraction
B cells naive
B cells memory
Plasma cells
T cells CD8
T cells CD4 naive
T cells CD4 memory resting
T cells CD4 memory activated
T cells follicular helper
T cells regulatory (Tregs)
T cells gamma delta
NK cells resting
NK cells activated
Monocytes
Macrophages M0
Macrophages M1
Macrophages M2
Dendritic cells resting
Dendritic cells activated
Mast cells resting
Mast cells activated
Eosinophils
Neutrophils
D
PDCD1
cor = 0.356
p = 1.58e−12
NCAPD2
Expression Level (log2 TPM)
E
CTLA4
cor = 0.318
p = 3.81e−10
F
Purity
B Cell
CD8+ T Cell
CD4+ T Cell
Macrophage
Neutrophil
Dendritic Cell
LIHC
NCAPD2 Expression Level (log2 TPM)
Infiltration Level
G
LIHC
Infiltration Level
Copy Number
Arm−level Deletion
Diploid/Normal
Arm−level Gain
High Amplication

Figure 10. Correlation between NCAPD2 expression and immune immunomodulatory genes and TME immune infiltration. A. The relationship between NCAPD2 expression and pan-cancer immune checkpoints. B. The relationship between NCAPD2 expression and pan-cancer immunomodulatory genes. C. The infiltrated landscape of 22 immune cells in HCC with differential expression of NCAPD2. D. Correlation between NCAPD2 and PDCD1. E. Correlation between NCAPD2 and CTLA4. F. The relationship between NCAPD2 expression and TME immune cells infiltration. G. The relationship between immune cells infiltration and different CNAs types of NCAPD2. $^{*}P < 0.05$, $^{**}P < 0.01$.

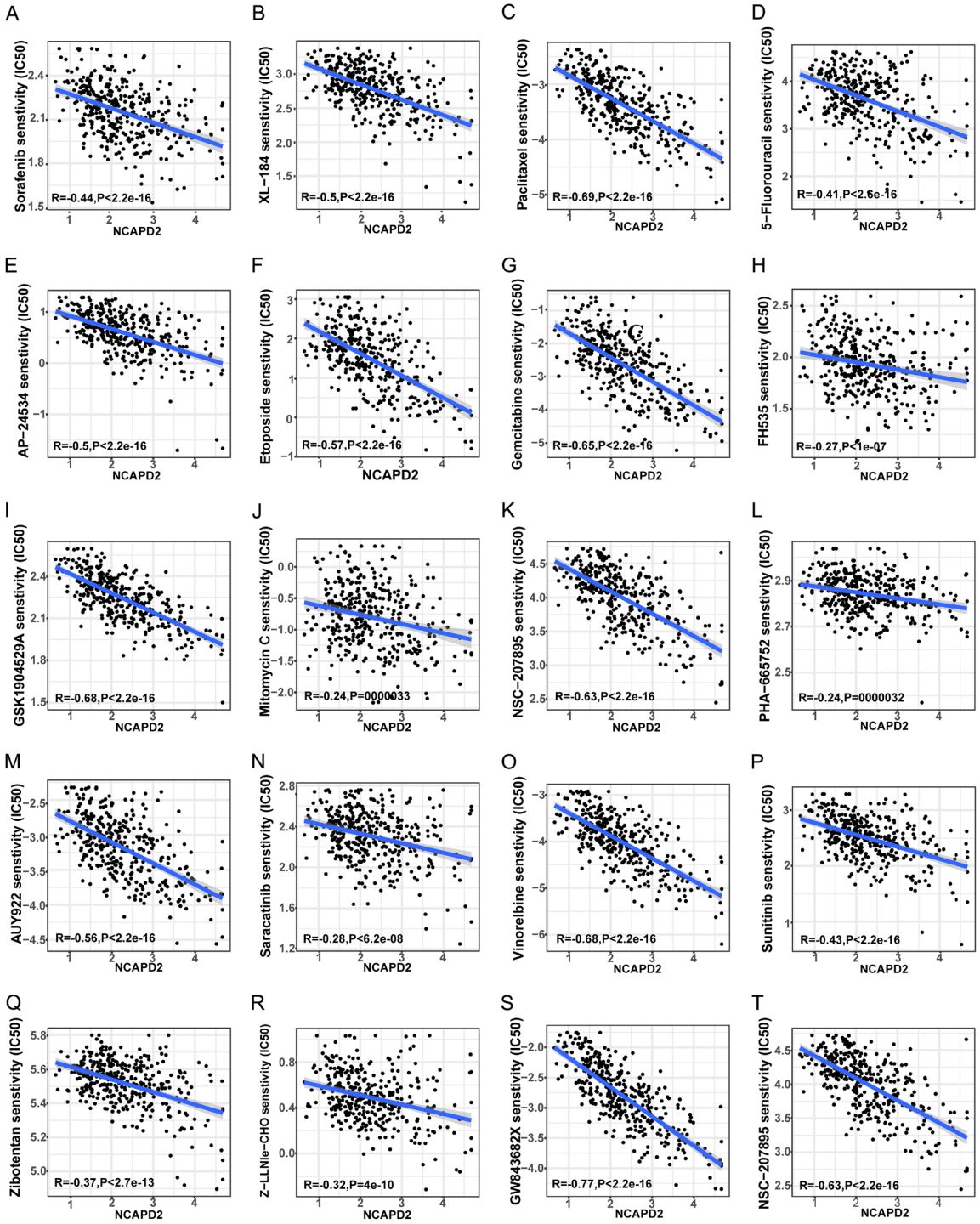

Figure 11. NCAPD2 was negatively correlated with the IC_{50} values of anticancer drugs. A-T. Detailed correlation analysis of 20 drug sensitivity and differential NCAPD2 expression.

treatment, exhibit higher sensitivity in groups with high NCAPD2 expression.

Discussion

HCC is a complex disease characterized by a poor prognosis and involves various molecular mechanisms. Epidemiological studies have shown that DM more than doubles the risk of hepatocarcinogenesis across different populations [5, 22, 23]. However, the underlying mechanisms remain to be elucidated. Thus, uncovering novel interactions between these two conditions could potentially enhance therapeutic effectiveness and improve the prognosis for HCC patients with concurrent DM.

Cancer cells require substantial energy to support rapid growth and expansion, primarily derived from glucose. Therefore, metabolic disorders such as persistent hyperglycemia, a hallmark of DM, are recognized as significant contributors to the onset and progression of HCC. Previous literature has underscored the role of hyperglycemia in the poor prognosis of HCC patients with DM, noting that reducing blood glucose levels can improve patient survival. High glucose levels are known to promote the proliferation, migration, and invasion of HCC cells, whereas glucose deprivation or reduction through metformin inhibits these malignant behaviors. Additionally, high glucose has been reported to trigger EMT, facilitating the malignant behaviors of several tumors through aberrant regulation of oncogenes or signaling pathways. Our findings corroborate evidence that high glucose (25 mmol/L) enhances the proliferation, migration, and invasion of HCC cells and promotes EMT progression compared to cells cultured in low glucose (5.6 mmol/L). However, the molecular mechanisms linking hyperglycemia-induced EMT to HCC remain to be fully elucidated.

NCAPD2, a regulatory subunit of the condensin I complex, was initially implicated in chromosome condensation and segregation and has recently been identified as a cancer promoter. Aberrant overexpression of NCAPD2 has been recognized as a prognostic factor in colorectal and breast cancers [19, 20]. Bioinformatic analyses based on RNA-seq data from public databases have also shown frequent overexpression of NCAPD2 in various tumors [21, 24]. However, the expression pattern and clinical significance of NCAPD2 in HCC patients, particularly those with DM, need further exploration. We confirmed the overexpression of NCAPD2 in HCC tumor tissues, which positively correlates with poor clinicopathological features and prognosis in both our local cohorts and multiple public databases, supporting its oncogenic role in HCC. DNA methylation, a common epigenetic modification, affects chromatin structure, DNA conformation, DNA stability, and DNA-protein interactions, thereby controlling gene expression and playing a critical role in tumorigenesis and progression of various cancers [25]. Decreased DNA methylation leads to reduced gene expression, while demethylation can reactivate gene expression. Consistently, we observed a lower promoter methylation of NCAPD2 in HCC tumor compared to normal tissues, which may explain the aberrant overexpression of NCAPD2 in HCC. Somatic mutation is another factor contributing to tumorigenesis and the poor prognosis of HCC patients [26]. We observed a 6% genetic alteration rate of NCAPD2 in HCC. TP53, a key tumor suppressor implicated in HCC, is closely related to HCC development [27]. Our results showed that TP53 mutation frequency was higher in HCC tumors than in normal tissues, with a 38% mutation frequency observed in the high NCAPD2 expression group and only 14% in the low NCAPD2 expression group. Notably, subgroup analysis of local clinical samples revealed significantly higher NCAPD2 expression in HCC patients with DM than those without, suggesting NCAPD2 as a critical link between HCC and DM and a poor prognostic indicator for HCC patients. DNA methylation and genetic alterations may be primary factors behind the aberrant expression and impact of NCAPD2 on HCC progression.

EMT is a common process observed in various tumors. Epithelial tumor cells undergoing EMT acquire aggressive mesenchymal traits, enabling them to migrate from the primary site to distant metastatic sites by altering their cytoskeleton and structure [28-31]. During EMT, the expression of epithelial biomarkers such as E-cadherin is suppressed while the specific proteins representing mesenchymal features accumulate [32]. Previous studies revealed that NCAPD2 blocked autophagic flux to exert tumor promoter effects in colorectal cancer via the Ca^{2+}/CAMKK/AMPK/mTORC1

pathway and PARP-1/SIRT1 [19]. NCAPD2 facilitated the progression of breast cancer by interacting with E2F1 to activate the transcriptional activity of CDK1 [20]. Based on bioinformatics analysis, previous studies have suggested that NCAPD2 primarily regulates the cell cycle in liver cancer, though empirical validation has been limited [24].

In this study, we provided evidence of a novel mechanism by which NACPD2 is involved in the regulation of EMT in HCC. Accompanied by changes in EMT markers, our experiments confirmed that knockdown of NCAPD2 suppressed malignant behaviors and EMT under high glucose conditions. We found that NCAPD2 was closely associated with the Wnt/β-catenin signaling pathway. There is a growing body of evidence suggesting that activation of the Wnt/β-catenin pathway promotes cell proliferation, migration, and stem cell renewal, contributing to the malignant progression of various cancers [11, 12]. β-catenin, which forms tight intercellular adhesions with E-cadherin, serves as a key transcriptional coactivator in the canonical Wnt signaling pathway by translocating from the cytoplasm to the nucleus to bind to TCF1/LEF1 [9]. The loss of E-cadherin disrupts the focal adhesion junction between E-cadherin and β-catenin, resulting in an increase of cell mobility. Moreover, the activation of downstream target genes such as CyclinD1, MMP7, and c-Myc has been implicated in promoting tumor growth by regulating cell cycle, apoptosis, or extracellular matrix remodeling [33]. Importantly, the translocation of β-catenin into the nucleus activates the Wnt/β-catenin signaling pathway, thereby triggering the EMT process [28]. Reportly, the translocation of β-catenin into cell nucleus activates the Wnt/β-catenin signaling pathway, thus triggering the EMT process [34]. Furthermore, studies have indicated that overexpression of LRP16 blocks the nuclear entry of β-catenin, regulating Wnt/β-catenin signaling to inhibit tumor growth in HCC [35]. Our study demonstrated that NCAPD2 knockdown reduced the expression of key components in the Wnt/β-catenin signaling pathway and decreased the nuclear entry of β-catenin, as shown by immunofluorescence experiments, suggesting that NCAPD2 promotes HCC progression and EMT through the regulation of Wnt/β-catenin signaling. Consistently, functional enrichment analysis in our study highlighted NCAPD2-mediated cell cycle regulation. Additionally, the PPI network we constructed revealed that NCAPD2 primarily interacts with NCAPDG, which has been reported to promote tumor progression by facilitating EMT via Wnt/β-catenin signaling [36, 37], further supporting a potential mechanism of NCAPD2 acting through the Wnt signaling pathway in HCC.

Due to the complexity of HCC, the efficacy of current treatment modalities remains relatively limited. Recent treatments based on immune checkpoints (ICPs) have emerged as significant breakthroughs in cancer therapy [38]. The complex tumor immune microenvironment (TME) plays a crucial role in the response to immunotherapy and tumor progression. Chemokines are critical for immune response and progression of HCC by controlling the mobility and recruitment of immune cells to tumors. CX3CL1 has been reported to promote the metastasis of HCC by binding to its receptor CXCR3, facilitating the differentiation of monocytes into M2 macrophages [39]. The SOX9/CXCL5 axis contributes to the proliferation and invasion of HCC cells increasing the infiltration of neutrophils and macrophages [40]. We demonstrated a positive association between NCAPD2 expression and levels of CX3CL1 and CXCL5. Furthermore, NCAPD2 was strongly related to the infiltration of neutrophil and macrophage, suggesting a potential regulatory mechanism of NCAPD2 on HCC immune responses.

Another potential molecular mechanism contributing to poor prognosis in HCC patients with high NCAPD2 expression is bidirectional regulatory effects between EMT and the TME [41, 42]. EMT is reported to be involved in the activation of ICPs, including PD-1 and CTLA4, through suppressing immune cells infiltration or crosstalk with stromal immune cells [43, 44]. Conversely, immune or stromal cells in the TME have been shown to regulate EMT progression. For instance, it is reported that tumor-associated macrophages (TAMs) promote EMT, thereby facilitating HCC progression through Wnt2b/β-catenin/c-Myc signaling and glycolysis regulation [45]. An association between poor survival of HCC patients and increased macrophage density was observed [46]. M2 macrophages have also been reported to induce EMT through the secretion of various cytokines, and regula-

tory T (Treg) cells were more commonly found in mesenchymal layers [47, 48]. Additionally, cells with mesenchymal phenotype are less susceptible to attack by CD8+ T or natural killer (NK) cells, resulting in tumor progression [47, 49, 50]. In this study, we showed that NCAPD2 was positively associated with numerous ICPs (including PDCD1 and CTLA4) and immune cells infiltration by macrophages, CD8+ T, dendritic cell, and B cells, reinforcing the specific role of NCAPD2 in mediating communication between HCC prognosis and TME. Further experimental studies are needed to confirm the effects of NCAPD2 on TME and drug sensitivity in HCC.

Conclusion

In this study, we identified the overexpression of NCAPD2 in both HCC tumors and cell lines, particularly in cases of HCC accompanied by DM. NCAPD2 emerged as a critical regulator of the malignant behaviors of HCC cells under hyperglycemic conditions through the Wnt signaling pathway, revealing novel crosstalk between HCC and DM for the first time. NCAPD2 was associated with poor prognosis of HCC patients and was closely linked to the TME. Therefore, NCAPD2 presents itself as a novel, important therapeutic target for inhibiting the progression of HCC in clinical settings. Future studies involving larger patient cohorts are recommended to further investigate this crucial link.

Acknowledgements

This work was supported by the National Nature Science Foundation of China (No. 81902500), the China Post-Doctoral Science Foundation (2022MD723764), the Guangxi Natural Science Foundation (Nos. 2023GXNSFBA026108, 2024GXNSFAA999059, 2017JJA10238) and the Innovation Project of Guangxi Graduate Education (No. YCSW2023229).

Disclosure of conflict of interest

None.

Address correspondence to: Ganlu Deng, Department of Oncology, The First Affiliated Hospital of Guangxi Medical University, Nanning 530021, Guangxi, China. Tel: +86-15676132389; E-mail: dengganlu@gxmu.edu.cn; Yingfen Qin, Department of Endocrinology, The First Affiliated Hospital of Guangxi Medical University, Nanning 530021, Guangxi, China. Tel: +86-13607862619; E-mail: yingfenq@126.com

References

[1] Saeedi P, Petersohn I, Salpea P, Malanda B, Karuranga S, Unwin N, Colagiuri S, Guariguata L, Motala AA, Ogurtsova K, Shaw JE, Bright D and Williams R; IDF Diabetes Atlas Committee. Global and regional diabetes prevalence estimates for 2019 and projections for 2030 and 2045: results from the International Diabetes Federation Diabetes Atlas, 9th edition. Diabetes Res Clin Pract 2019; 157: 107843.

[2] Calderaro J, Seraphin TP, Luedde T and Simon TG. Artificial intelligence for the prevention and clinical management of hepatocellular carcinoma. J Hepatol 2022; 76: 1348-1361.

[3] Toh MR, Wong EYT, Wong SH, Ng AWT, Loo LH, Chow PK and Ngeow J. Global epidemiology and genetics of hepatocellular carcinoma. Gastroenterology 2023; 164: 766-782.

[4] Chen R, Li Q, Xu S, Ye C, Tian T, Jiang Q, Shan J and Ruan J. Modulation of the tumour microenvironment in hepatocellular carcinoma by tyrosine kinase inhibitors: from modulation to combination therapy targeting the microenvironment. Cancer Cell Int 2022; 22: 73.

[5] Pang Y, Kartsonaki C, Turnbull I, Guo Y, Clarke R, Chen Y, Bragg F, Yang L, Bian Z, Millwood IY, Hao J, Han X, Zang Y, Chen J, Li L, Holmes MV and Chen Z. Diabetes, plasma glucose, and incidence of fatty liver, cirrhosis, and liver cancer: a prospective study of 0.5 million people. Hepatology 2018; 68: 1308-1318.

[6] Tian Y, Yang B, Qiu W, Hao Y, Zhang Z, Yang B, Li N, Cheng S, Lin Z, Rui YC, Cheung OKW, Yang W, Wu WKK, Cheung YS, Lai PBS, Luo J, Sung JJY, Chen R, Wang HY, Cheng ASL and Yang P. ER-residential Nogo-B accelerates NAFLD-associated HCC mediated by metabolic reprogramming of oxLDL lipophagy. Nat Commun 2019; 10: 3391.

[7] Yoo JJ, Cho EJ, Han K, Heo SS, Kim BY, Shin DW and Yu SJ. Glucose variability and risk of hepatocellular carcinoma in patients with diabetes: a nationwide population-based study. Cancer Epidemiol Biomarkers Prev 2021; 30: 974-981.

[8] Huang Y, Hong W and Wei X. The molecular mechanisms and therapeutic strategies of EMT in tumor progression and metastasis. J Hematol Oncol 2022; 15: 129.

[9] Guo F, Wang H, Jiang M, Yang Q, Xiang Q, Zhou H, Hu X, Hao K, Yang J, Cao H and Shen Z. TDP-43 induces EMT and promotes hepatocellular carcinoma metastasis via activating Wnt/β-catenin signaling pathway. Am J Cancer Res 2020; 10: 3285-3301.

[10] Santos JM and Hussain F. Higher glucose enhances breast cancer cell aggressiveness. Nutr Cancer 2020; 72: 734-746.
[11] Wu J, Chen J, Xi Y, Wang F, Sha H, Luo L, Zhu Y, Hong X and Bu S. High glucose induces epithelial-mesenchymal transition and results in the migration and invasion of colorectal cancer cells. Exp Ther Med 2018; 16: 222-230.
[12] Guo J, Ye F, Jiang X, Guo H, Xie W, Zhang Y and Sheng X. Drp1 mediates high glucose-induced mitochondrial dysfunction and epithelial-mesenchymal transition in endometrial cancer cells. Exp Cell Res 2020; 389: 111880.
[13] Chen YC, Ou MC, Fang CW, Lee TH and Tzeng SL. High glucose concentrations negatively regulate the IGF1R/Src/ERK axis through the microRNA-9 in colorectal cancer. Cells 2019; 8: 326.
[14] Li S, Zhu H, Chen H, Xia J, Zhang F, Xu R and Lin Q. Glucose promotes epithelial-mesenchymal transitions in bladder cancer by regulating the functions of YAP1 and TAZ. J Cell Mol Med 2020; 24: 10391-10401.
[15] Sorin S, Zhou Y, Thithuan K, Khawkhiaw K, Zeng F, Ruangpratyakul T, Chomphoo S, Seubwai W, Wongkham S and Saengboonmee C. High glucose enhances the aggressiveness of lung adenocarcinoma via activating epidermal growth factor receptor/signal transducer and activator of transcription 3 pathways. J Nutr Biochem 2023; 119: 109399.
[16] Topel H, Bağırsakçı E, Yılmaz Y, Güneş A, Bağcı G, Çömez D, Kahraman E, Korhan P and Atabey N. High glucose induced c-Met activation promotes aggressive phenotype and regulates expression of glucose metabolism genes in HCC cells. Sci Rep 2021; 11: 11376.
[17] Zhang P, Liu L, Huang J, Shao L, Wang H, Xiong N and Wang T. Non-SMC condensin I complex, subunit D2 gene polymorphisms are associated with Parkinson's disease: a Han Chinese study. Genome 2014; 57: 253-257.
[18] Martin CA, Murray JE, Carroll P, Leitch A, Mackenzie KJ, Halachev M, Fetit AE, Keith C, Bicknell LS, Fluteau A, Gautier P, Hall EA, Joss S, Soares G, Silva J, Bober MB, Duker A, Wise CA, Quigley AJ, Phadke SR; Deciphering Developmental Disorders Study, Wood AJ, Vagnarelli P and Jackson AP. Mutations in genes encoding condensin complex proteins cause microcephaly through decatenation failure at mitosis. Genes Dev 2016; 30: 2158-2172.
[19] Jing Z, He X, Jia Z, Sa Y, Yang B and Liu P. NCAPD2 inhibits autophagy by regulating Ca2+/CAMKK2/AMPK/mTORC1 pathway and PARP-1/SIRT1 axis to promote colorectal cancer. Cancer Lett 2021; 520: 26-37.
[20] He J, Gao R, Yang J, Li F, Fu Y, Cui J, Liu X, Huang K, Guo Q, Zhou Z and Wei W. NCAPD2 promotes breast cancer progression through E2F1 transcriptional regulation of CDK1. Cancer Sci 2023; 114: 896-907.
[21] Li Z, Zheng Y, Wu Z, Zhuo T, Zhu Y, Dai L, Wang Y and Chen M. NCAPD2 is a novel marker for the poor prognosis of lung adenocarcinoma and is associated with immune infiltration and tumor mutational burden. Medicine (Baltimore) 2023; 102: e32686.
[22] Ohkuma T, Peters SAE and Woodward M. Sex differences in the association between diabetes and cancer: a systematic review and meta-analysis of 121 cohorts including 20 million individuals and one million events. Diabetologia 2018; 61: 2140-2154.
[23] Koh WP, Wang R, Jin A, Yu MC and Yuan JM. Diabetes mellitus and risk of hepatocellular carcinoma: findings from the Singapore Chinese Health Study. Br J Cancer 2013; 108: 1182-1188.
[24] Dong X, Liu T, Li Z and Zhai Y. Non-SMC condensin I complex subunit D2 (NCAPD2) reveals its prognostic and immunologic features in human cancers. Aging (Albany NY) 2023; 15: 7237-7257.
[25] Wang J, Yang J, Li D and Li J. Technologies for targeting DNA methylation modifications: basic mechanism and potential application in cancer. Biochim Biophys Acta Rev Cancer 2021; 1875: 188454.
[26] De Stefano F, Chacon E, Turcios L, Marti F and Gedaly R. Novel biomarkers in hepatocellular carcinoma. Dig Liver Dis 2018; 50: 1115-1123.
[27] Zhou Y, Cui G, Xu H, Chun J, Yang D, Zhang Z, Yang L, Wang J, Wan M, Calvisi DF, Lin S, Chen X and Wang H. Loss of TP53 cooperates with c-MET overexpression to drive hepatocarcinogenesis. Cell Death Dis 2023; 14: 476.
[28] Xu X, Zhang Y, Wang X, Li S and Tang L. Substrate stiffness drives epithelial to mesenchymal transition and proliferation through the NEAT1-Wnt/β-Catenin pathway in liver cancer. Int J Mol Sci 2021; 22: 12066.
[29] Banyard J and Bielenberg DR. The role of EMT and MET in cancer dissemination. Connect Tissue Res 2015; 56: 403-413.
[30] Aiello NM and Kang Y. Context-dependent EMT programs in cancer metastasis. J Exp Med 2019; 216: 1016-1026.
[31] Lu W and Kang Y. Epithelial-mesenchymal plasticity in cancer progression and metastasis. Dev Cell 2019; 49: 361-374.
[32] Orrapin S, Udomruk S, Lapisatepun W, Moonmuang S, Phanphaisarn A, Phinyo P, Pruksakorn D and Chaiyawat P. Clinical implication of circulating tumor cells expressing epithelial mesenchymal transition (EMT) and cancer stem cell (CSC) markers and their perspective

in HCC: a systematic review. Cancers (Basel) 2022; 14: 3373.
[33] Khanam A and Kottilil S. New therapeutics for HCC: does tumor immune microenvironment matter? Int J Mol Sci 2022; 24: 437.
[34] Wang H and Zhang P. lncRNA-CASC15 promotes osteosarcoma proliferation and metastasis by regulating epithelial-mesenchymal transition via the Wnt/β-catenin signaling pathway. Oncol Rep 2021; 45: 76.
[35] Shao L, Jing W, Wang L, Pan F, Wu L, Zhang L, Yang P, Hu M and Fan K. LRP16 prevents hepatocellular carcinoma progression through regulation of Wnt/β-catenin signaling. J Mol Med (Berl) 2018; 96: 547-558.
[36] Shi Y, Ge C, Fang D, Wei W, Li L, Wei Q and Yu H. NCAPG facilitates colorectal cancer cell proliferation, migration, invasion and epithelial-mesenchymal transition by activating the Wnt/β-catenin signaling pathway. Cancer Cell Int 2022; 22: 119.
[37] Zhang X, Zhu M, Wang H, Song Z, Zhan D, Cao W, Han Y and Jia J. Overexpression of NCAPG inhibits cardia adenocarcinoma apoptosis and promotes epithelial-mesenchymal transition through the Wnt/β-catenin signaling pathway. Gene 2021; 766: 145163.
[38] Foerster F, Gairing SJ, Ilyas SI and Galle PR. Emerging immunotherapy for HCC: a guide for hepatologists. Hepatology 2022; 75: 1604-1626.
[39] Sun C, Hu A, Wang S, Tian B, Jiang L, Liang Y, Wang H and Dong J. ADAM17-regulated CX-3CL1 expression produced by bone marrow endothelial cells promotes spinal metastasis from hepatocellular carcinoma. Int J Oncol 2020; 57: 249-263.
[40] Ren Z, Chen Y, Shi L, Shao F, Sun Y, Ge J, Zhang J and Zang Y. Sox9/CXCL5 axis facilitates tumour cell growth and invasion in hepatocellular carcinoma. FEBS J 2022; 289: 3535-3549.
[41] Liu Y, Xun Z, Ma K, Liang S, Li X, Zhou S, Sun L, Liu Y, Du Y, Guo X, Cui T, Zhou H, Wang J, Yin D, Song R, Zhang S, Cai W, Meng F, Guo H, Zhang B, Yang D, Bao R, Hu Q, Wang J, Ye Y and Liu L. Identification of a tumour immune barrier in the HCC microenvironment that determines the efficacy of immunotherapy. J Hepatol 2023; 78: 770-782.
[42] Erin N, Grahovac J, Brozovic A and Efferth T. Tumor microenvironment and epithelial mesenchymal transition as targets to overcome tumor multidrug resistance. Drug Resist Updat 2020; 53: 100715.
[43] Jiang Y and Zhan H. Communication between EMT and PD-L1 signaling: new insights into tumor immune evasion. Cancer Lett 2020; 468: 72-81.
[44] Taki M, Abiko K, Ukita M, Murakami R, Yamanoi K, Yamaguchi K, Hamanishi J, Baba T, Matsumura N and Mandai M. Tumor immune microenvironment during epithelial-mesenchymal transition. Clin Cancer Res 2021; 27: 4669-4679.
[45] Jiang Y, Han Q, Zhao H and Zhang J. Promotion of epithelial-mesenchymal transformation by hepatocellular carcinoma-educated macrophages through Wnt2b/β-catenin/c-Myc signaling and reprogramming glycolysis. J Exp Clin Cancer Res 2021; 40: 13.
[46] Li X, Yao W, Yuan Y, Chen P, Li B, Li J, Chu R, Song H, Xie D, Jiang X and Wang H. Targeting of tumour-infiltrating macrophages via CCL2/CCR2 signalling as a therapeutic strategy against hepatocellular carcinoma. Gut 2017; 66: 157-167.
[47] Dongre A, Rashidian M, Reinhardt F, Bagnato A, Keckesova Z, Ploegh HL and Weinberg RA. Epithelial-to-mesenchymal transition contributes to immunosuppression in breast carcinomas. Cancer Res 2017; 77: 3982-3989.
[48] Chen Y, Tan W and Wang C. Tumor-associated macrophage-derived cytokines enhance cancer stem-like characteristics through epithelial-mesenchymal transition. Onco Targets Ther 2018; 11: 3817-3826.
[49] Nieto MA, Huang RY, Jackson RA and Thiery JP. EMT: 2016. Cell 2016; 166: 21-45.
[50] Zhan HX, Zhou B, Cheng YG, Xu JW, Wang L, Zhang GY and Hu SY. Crosstalk between stromal cells and cancer cells in pancreatic cancer: new insights into stromal biology. Cancer Lett 2017; 392: 83-93.

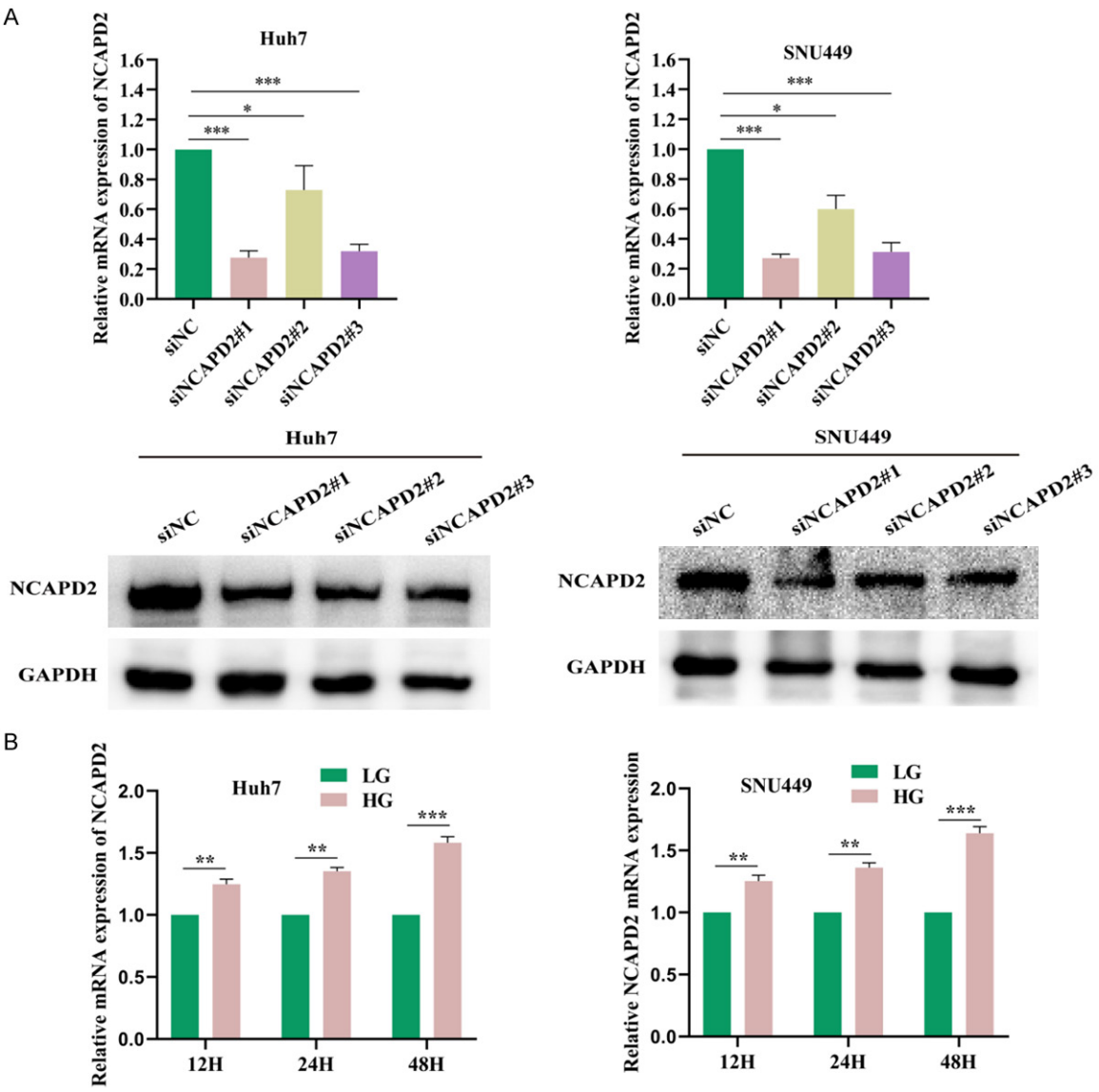

Supplementary Figure 1. A. The transfection efficiency of siRNAs was detected and confirmed by qRT-PCR and Western blot. B. qRT-PCR assay showed a time-dependent increase in the mRNA expression of NCAPD2 in HG groups as compared with cells grown in LG. $^{*}P < 0.05$, $^{**}P < 0.01$, $^{***}P < 0.001$.